TELSEM: a Tool to Estimate Land Surface Emissivities at Microwave frequencies

Version 1.0

November 2009

EUMETSAT

NWP SAF

Table of Contents

1. Introduction

1.1. Scope of the document

This document describes a microwave emissivity interpolator attached to RTTOV, along with the emissivity climatology to which it is anchored. It provides the necessary technical information for the user who wishes to use this tool.

1.2. Software version identification

The current version of the softwave is 1.0.

2. Description of the MW emissivity interpolator

2.1. Goal of the Emissivity interpolator

The goal of the emissivity interpolator is to provide a first-guess of the microwave emissivity for simulation purposes of MW satellite observations, for its use in inversion algorithms, and as a tool for variational assimilation.

The interpolator is originally designed for frequencies between 19 and 85 GHz. However, it can still be used for lower or higher frequencies. Tests have shown that it is beneficial down to 10 GHz or up to 190 GHz. For example, it has been shown very valuable at AMSU-B frequencies.

2.2. SSM/I MW emissivity dataset description

The interpolator is anchored to a monthly-mean climatology of emissivities calculated from SSM/I observations at SSM/I frequencies (19, 22, 37 and 85 GHz for vertical and horizontal polarizations, except for 22 GHz which is vertical only), with a spatial resolution of 0.25°x0.25° at the equator (equal area grid). This climatology has been computed by averaging 8 years of SSM/I monthly-mean emissivities (from 1993 to 2000, see references in annexe 1). This climatology is distributed with the emissivity interpolator. The ASCII files content is described in the following table:

Cell number	Number of the cell in the 0.25°×0.25° equal-area grid
Emis19V	Emissivity at 19 GHz for vertical polarization
Emis19H	Emissivity at 19 GHz for horizontal polarization
Emis22V	Emissivity at 22 GHz for vertical polarization
Emis37V	Emissivity at 37 GHz for vertical polarization
Emis37H	Emissivity at 37 GHz for horizontal polarization
Emis85V	Emissivity at 85 GHz for vertical polarization
Emis85H	Emissivity at 85 GHz for horizontal polarization
VAR Emis19V	Variance[1] of the emissivity at 19 GHz V used as uncertainty
VAR Emis19H	Variance of the emissivity at 19 GHz H used as uncertainty

---

[1] Please note that the original climatology files provide the variance of the emissivity uncertainties but that the interpolator converts right away, during the reading of this to the emissivity uncertainty standard-deviation.

VAR Emis22V	Variance of the emissivity at 22 GHz V used as uncertainty
VAR Emis37V	Variance of the emissivity at 37 GHz V used as uncertainty
VAR Emis37H	Variance of the emissivity at 37 GHz H used as uncertainty
VAR Emis85V	Variance of the emissivity at 85 GHz V used as uncertainty
VAR Emis85H	Variance of the emissivity at 85 GHz H used as uncertainty
Surface class	Surface class for the location: from 1 to 5 snow and ice free regions from highly vegetated to desert, from 6 to 9 various snow and ice types, and class 10 for pixels containing standing water.

A file (correlations.txt) is also distributed to provide the 7×7 correlation matrices of the SSM/I emissivity uncertainties.

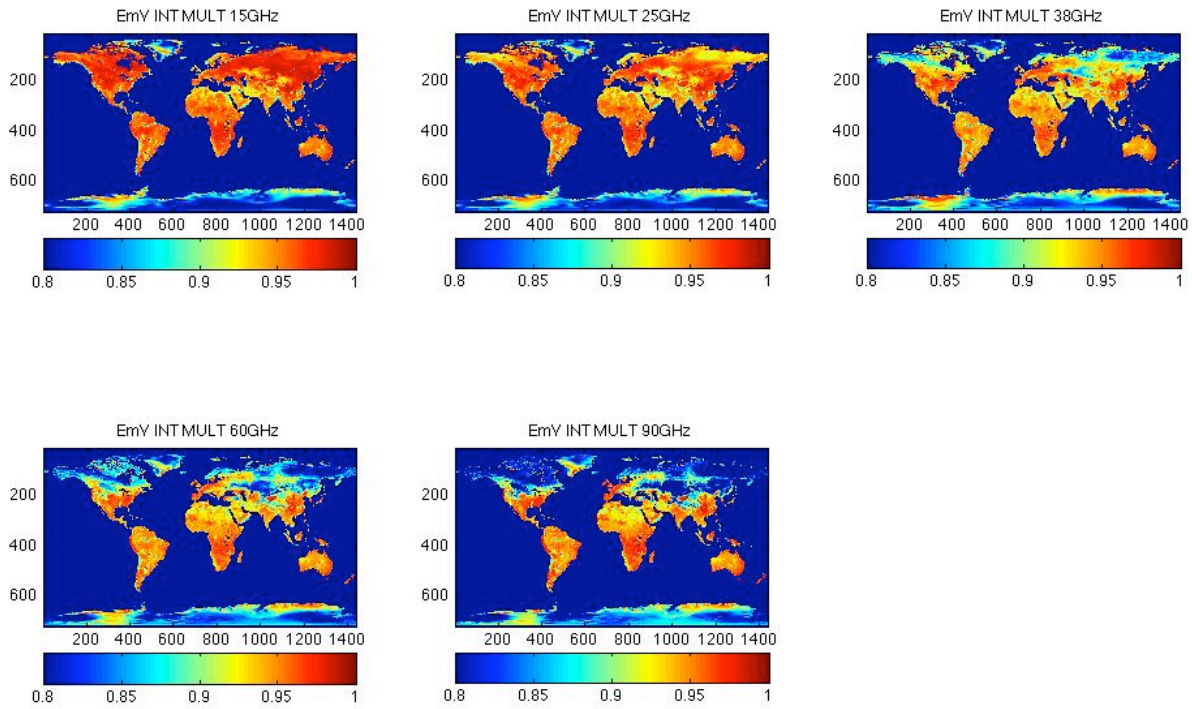### 2.3. Interpolation scheme description
See annexe 3.

2.4. Different configurations for the interpolator
Four configurations have been considered for the emissivity interpolator to facilitate and optimize its use, depending on the various applications that can utilize the interpolator. These 4 configurations are:
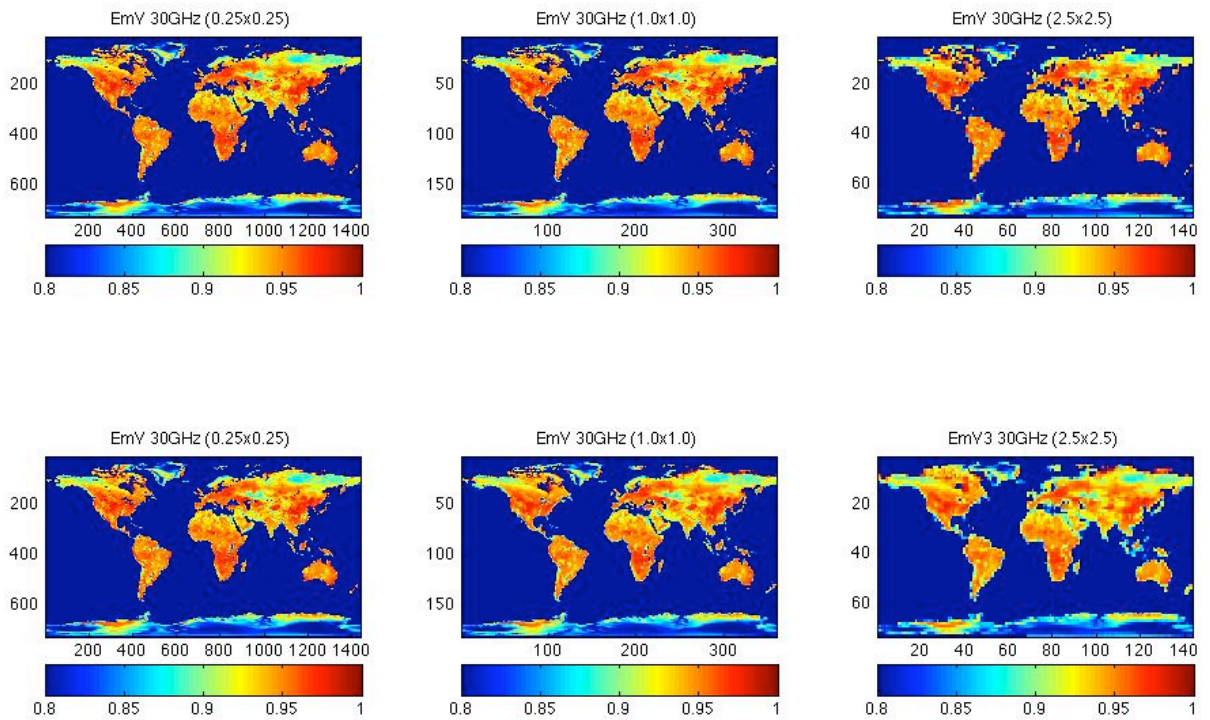
- **IND_SING**: when the location and frequency are specified, the interpolator uses an INDividual atlas-pixel (i.e. nearest location in the equal-are grid), and estimates a SINGle frequency emissivity.
  → *emis_interp_ind_sing*(lat, lon, theta, freq, atlas, ev, eh, stdv, stdh, verb)

- **INT_SING**: In this configuration again, only one frequency is considered but the interpolator INTegrates multiple atlas pixels taking into account the resolution that is specified. If the spatial resolution is higher than the 0.25° x0.25° spatial resolution of the initial dataset, the pixels that fall into the new spatial grids are averaged. If the spatial resolution is lower than the 0.25°x0.25° initial spatial resolution, the nearest pixel is considered.
  → *emis_interp_int_sing*(lat, lon, resol, theta, freq, atlas, ev, eh, stdv, stdh, verb)

- **IND_MULT**: The nearest atlas-pixel is used here to interpolate at MULTiple frequencies.
  → *emis_interp_ind_mult*(lat, lon, theta, freq, n_chan, atlas, ev, eh, std, verb)

- **INT_MULT**: The INTegration of the atlas-pixels is used to interpolate MULTiple frequencies.
  → *emis_interp_int_sing*(lat, lon, resol, theta, freq, atlas, ev, eh, std, verb)

2.5. Examples of interpolated emissivities
In the following figures, the INT_MULT interpolator configuration is used to estimate the emissivities at 15, 25, 38, 60 and 90 GHz at vertical polarization.

EmY INT MULT 15GHz   EmY INT MULT 25GHz   EmY INT MULT 38GHz

EmY INT MULT 60GHz   EmY INT MULT 90GHz

The next figures give examples of emissivity estimates for 30 GHz at vertical polarization for horizontal resolutions, from left to right, of 0.25°×0.25°, 1.0°×1.0° and 2.5°×2.5°; top 3 maps are for the IND configuration (nearest atlas-pixels), and bottom 3 maps are for the INT configuration (i.e., integration of the atlas pixels).

EmY 30GHz (0.25x0.25)   EmY 30GHz (1.0x1.0)   EmY 30GHz (2.5x2.5)

EmY 30GHz (0.25x0.25)   EmY 30GHz (1.0x1.0)   EmY3 30GHz (2.5x2.5)

2.6. Interpolation of the uncertainties

Let $EM_{SSMI}(6)$ be the 6-channels SSM/I emissivities from the atlas (19V, 37V, 85V, 19H, 37H and 85H). The goal of the emissivity interpolator is to estimate a new emissivities $EM_{NEW}(f)$ at frequency f. The first half of EM_{NEW} is for vertical and the second half for horizontal polarizations. How is the new uncertainty covariance matrices computed?

In order to estimate the emissivities at new frequencies (and scanning angle and polarization), the interpolator uses a (f×6) matrix, FIM, such that:

$$(EmV; EmH) = FIM \bullet EM_{SSMI}$$

From the SSMI atlas, we have the 6×6 correlation matrix:

$$COR_{SSMI}(6,6)$$

for the uncertainties on the 6 SSMI channels and the associated vector of uncertainty standard deviation is defined by:

$$STD_{SSMI}(6)$$

The covariance matrix of the new emissivity uncertainties can be estimated using:

$$COV_{SSMI} = STD'_{SSMI} \bullet COR_{SSMI} \bullet STD_{SSMI}$$

The covariance matrix of the new emissivity uncertainties can be estimated using:

$$COV_{NEW} = FIM' \bullet COV_{SSMI} \bullet FIM = FIM' \bullet STD'_{SSMI} \bullet COR_{SSMI} \bullet STD_{SSMI} \bullet FIM$$

In order to better explain this process, an example of such computations is given in Annexe 2.

The following figure gives the uncertainty estimates for interpolation at 15, 25, 38, 60 and 90 GHz.

2.7. List of inputs/outputs for the interpolator

Real Latitude: [-90; 90]

Real Longitude: [0; 360]

Real Theta [0; 60°]   *! Incidence angle*

Real freq[19; 85]   *!(in GHz) Freq to interpolate. It is possible to use lower/higher freq.*

! -----For individual freq interpolations

Real ev, eh, stdv, stdh   *! Interpolated emissivities with uncertainties (emis are between 0-1)*

!----- For multiple freq interpolations

Real resol   *! Horizontal resolution for the user*

Integer n_chan=5   *!Number of channel to interpolate*

Real ev(5), eh(5), std(2*5,2*5)   *!Interpolated emissivities with uncertainties*

Real freq2(5)   *!Frequencies for the interpolation*

2.8. Implementation of the interpolator

2.8.1. Installation

The atlas (12 monthly-mean emissivity files and the correlations file) can be copied in any location. The library needs to be compiled with

> g95 -c mod_mwatlas.f90

The compilation of the Fortran code, *test*, that will ask for the library needs to be compiled with:

> g95 -o test mod_mwatlas.o test.o

A make file is provided (make, make clean, make test). The user needs to edit the makefile code to for their local compiler and flags.

The make test launches a ndiff command to verify that the computation done by the interpolator is similar to a test_reference case (see makefile). To this purpose, the user needs to check that the "ndiff" command is installed in its machines (this is similar to the usual "diff" command but with the possibility to introduce a threshold).

The compilation has been tested using Nag, g95, gFortran et Ifort compilers on Linux and Mac machines (64bytes).

2.8.2. Structure of the library

At the hart of the library is the structure Atlas_emis_mw that represents the microwave emissivity atlas. This structure is composed by:

TYPE atlas_emis_mw		
Type	**Array name**	**Contents**
INTEGER	Ndat	Number of lines in the atlas
INTEGER	Nchan	Number of channels in the atlas
CHARACTER(len=22)	Name	Name of the atlas (including version number)
INTEGER	Month	Month of the atlas
REAL	Dlat	Resolution of the atlas (equal-area)
INTEGER, POINTER	ncells(:)	Number of cells per lat band
INTEGER, POINTER	Firstcell(:)	The first cell number of lat band
REAL	lat1, lat2, lon1, lon2	Limits of the spatial domain (flagged if global)
REAL, POINTER	emis(ndat,nchan)	Emissivities
REAL, POINTER	correl(10,nchan,nchan)	Correlations or uncertainties for each surface class
REAL, POINTER	emis_err(ndat,nchan)	Emissivity uncertainties (std)
INTEGER, POINTER	class(ndat)	Surface class (1-10)
INTEGER, POINTER	Cellnum(ndat)	Cell number of each pixel in the atlas
INTEGER	correspondance(660066)	"Correspondance" vector indicating

		that for the ith element, the j so that EMIS(j,...) is the emissivity of cell number i.

The codes are in a library « mod_mwatlas.f90 ».

- SUBROUTINE **rttov_readmw_atlas**(dir,month,atlas,error_status,lat1,lat2,lon1,lon2)
  These routines read the emissivity atlas, including the emissivities, the associated standard deviations for uncertainties and the correlation matrices for uncertainties for each surface type (see files in section 2.2). The user can specify a zone (lat1, lat2, lon1 and lon2) to download only a limited amount of the atlas.

- SUBROUTINE **equare**(DLAT,NCELLS,FIRSTCELL)
  This routine computes the number of cells and the first cell number for each latitude band. This procedure is for equal-area grids such as for the SSM/I microwave atlas provided in this package. As an example, for a $0.25° \times 0.25°$ equal-area grid, there are 720 latitude bands, NCELLS(720) gives the numbers of pixels for each band, and FIRSTCELL(720) gives the cell number of the first pixel in a latitude band.

- FUNCTION **calc_cellnum**(lat,lon,atlas)
  This routine computes the cell number from the lat and lon. This procedure uses the NCELLS included in the atlas, and computed once and for all by routine EQUARE during the atlas reading (rttov_readmw_atlas).

- SUBROUTINE **calc_cellnum_mult**(lat,lon,resol,atlas,cell_num_mult,nb_cell)
  This routine is similar to function CALC_CELLNUM but it computes the list of cell numbers from the latitude, longitude and resolution (desired spatial resolution of the outputs). Gives for each cell of the new grid the cell numbers of the pixels in the initial grid to be averaged. This routine uses the NCELLS and FIRSTCELLS included in the atlas.

- SUBROUTINE **interp_freq2**(emiss19,emiss37,emiss85,f,emiss,an,bn,cn)
  This routine computes the linear interpolation of emissivity given the frequency and the atlas values for that cell number.

- SUBROUTINE **emis_interp**(lat,lon,theta,freq,classe,ev,eh,emiss_interp_v,emiss_interp_h)
  This routine performs the interpolation of emissivity in angle and frequency.

- SUBROUTINE **emis_interp_ind_sing**(lat,lon,theta,freq,atlas,ev,eh,stdv,stdh,verb)
  Interpolates emissivity for:
      IND: individual atlas-pixel
      SING: singular channel

- SUBROUTINE **emis_interp_int_sing**(lat,lon,resol,theta,freq,atlas,ev,eh,stdv,stdh,verb)
  Interpolates emissivity for:
      INT: integrate atlas-pixel
      SING: singular channel

- SUBROUTINE **emis_interp_ind_mult**(lat,lon,theta,freq,n_chan,atlas,ev,eh,std,verb)
  Interpolates emissivity for:
      IND: individual cell number atlas-pixel
      MULT: multiple channel

- SUBROUTINE **emis_interp_int_mult**(lat,lon,resol,theta,freq,atlas,ev,eh,std,verb)
  Interpolates emissivity for:
      INT: integrate atlas-pixel

MULT: multiple channel

2.8.3. Execution step
Please, see example in file test.f90

Annexe 1: References

- Prigent, C., E. Jaumouille, F. Chevallier, and F. Aires, A parameterization of the microwave land surface emissivity between 19 and 100 GHz, anchored to satellite-derived estimates, IEEE TGRS, 46, 344-352, 2008.
- Prigent, C., F. Aires, and W. B. Rossow, Land surface microwave emissivities over the globe for a decade, Bul. Amer. Meteorol. Soc., doi:10.1175/BAMS-87-11-1573, 1573-1584, 2006.
- Prigent, C., Microwave emissivity in arid reagions, what can we learn from satellite observations?, Chap. 4.5 in "Thermal Microwave Radiation - Applications for Remote Sensing", Matzler, C., P.W. Rosenkranz, A. Battaglia, and J.P. Wigneron (eds.), IEE Electromagnetic Waves Series 52, London, UK, 2006.
- Prigent, C., Passive microwave emissivity in vegetated reagions as directly calculated from satellite observations, Chap. 4.6, in "Thermal Microwave Radiation - Applications for Remote Sensing", Matzler, C., P.W. Rosenkranz, A. Battaglia, and J.P. Wigneron (eds.), IEE Electromagnetic Waves Series 52, London, UK, 2006.
- Prigent, C., J. Munier, B. Thomas, and G. Ruffié, Microwave signatures over carbonate sedimentary platforms in arid areas: Potential geological applications of passive microwave observations?, Geophys. Res. Let., 32, L23405, doi:10.1029/2005GL024691, 2005.
- Karbou, F., and C. Prigent, Calculation of microwave land surface emissivity from satellite observations: validity of the specular approximation over snow-free surfaces? IEEE Geoscience Remote Sensing Letters, 2, 311-314, 2005.
- Prigent, C., F. Chevallier, F. Karbou, P. Bauer and G. Kelly, AMSU-A land surface emissivity estimation for numerical weather prediction assimilation schemes, Journal of Applied Meteorology, 44, 416-426, 2005.
- Karbou, F., C. Prigent, L. Eymard, and J. Pardo, Microwave land emissivity calculations using AMSU measurements, IEEE TGRSE, 43, 5, 948- 959, 2005.
- Aires, F., C. Prigent, W. B. Rossow, M. Rothstein, A new neural network approach including first-guess for retrieval of atmospheric water vapor, cloud liquid water path,surface temperature and emissivities over land from satellite microwave observations, Journal of Geophysical Research, 106, 14 887-14 907, 2001.
- Prigent, C., J.P. Wigneron, W. B. Rossow, J. R. Pardo-Carrion, Frequency and angular variations of land surface microwave emissivities: Can we estimate SSM/T and AMSU emissivities from SSM/I emissivities?, IEEE Transactions on Geoscience and Remote Sensing, 38, 2373-2386, 2000.
- Prigent, C., W. B. Rossow, E.Matthews, Global maps of microwave land surface emissivities: Potential for land surface characterization, Radio Science, 33, 745-751, 1998.
- Prigent C., W. B. Rossow, E. Matthews, Microwave land surface emissivities estimated from SSM/I observations, Journal of Geophysical Research, 102, 21867-21890, 1997.

Annexe 2: Example for uncertainty calculations

How are the uncertainty covariance matrices computed? The emissivities for new frequencies are first computed:

Frequency	15 GHz	25 GHz	38 GHz	60 GHz	90 GHz
Emis V	0.9603142	0.9595809	0.9588379	0.9618543	0.9659674
Emis H	0.9590667	0.9586814	0.9583531	0.9613068	0.9653345

From the SSMI atlas, we have the 6x6 covariance matrix Cov_{SSMI} and the correlation matrix Cor_{SSMI} for the uncertainties on the 6 SSM/I channels (19, 37 and 85 GHz for both V and H polarizations).

Em19V	0.0004	0.0004	0.0004	0.0004	0.0004	0.0004
Em37V		0.0005	0.0004	0.0005	0.0005	0.0005
Em87V			0.0004	0.0004	0.0005	0.0005
Em19H				0.0005	0.0005	0.0005
Em37H					0.0010	0.0009
Em87H						0.0010

And the associated correlation matrix:

Em19V	**1.00**	0.96	0.96	0.94	0.72	0.73
Em37V		**1.00**	0.95	0.95	0.71	0.72
Em87V			**1.00**	0.96	0.79	0.79
Em19H				**1.00**	0.76	0.78
Em37H					**1.00**	0.93
Em87H						**1.00**

The "interpolation" matrix FIM is given by:

1.0000	0.0000	0.0000	0.0000	0.0000	0.0000
0.6799	**0.3201**	0.0000	0.0000	0.0000	0.0000
0.0000	**0.9794**	**0.0206**	0.0000	0.0000	0.0000
0.0000	**0.5258**	**0.4742**	0.0000	0.0000	0.0000
0.0000	0.0000	**1.0000**	0.0000	0.0000	0.0000
0.0000	0.0000	0.0000	**1.0000**	0.0000	0.0000
0.0000	0.0000	0.0000	**0.6799**	**0.3201**	0.0000
0.0000	0.0000	0.0000	0.0000	**0.9794**	**0.0206**
0.0000	0.0000	0.0000	0.0000	**0.5258**	**0.4742**
0.0000	0.0000	0.0000	0.0000	0.0000	**1.0000**

And the new covariance matrix is estimated by:

Cov=10^{-4}.

Em15V	4	4	4	4	4	4	4	4	4	4
Em25V		4	4	4	4	4	4	5	5	5
Em38V			5	5	4	5	5	5	5	5
Em60V				4	4	4	4	5	5	5
Em90V					4	4	4	5	5	5
Em15H						5	5	5	5	5
Em25H							5	7	7	7
Em38H								10	10	9
Em60H									10	10
Em90H										10

That corresponds to a correlation matrix:

Em15V	1.00	0.995	0.960	0.972	0.960	0.940	0.904	0.721	0.737	0.730
Em25V		1.00	0.983	0.987	0.965	0.952	0.913	0.724	0.741	0.733
Em38V			1.00	0.991	0.951	0.951	0.908	0.713	0.729	0.721
Em60V				1.00	0.984	0.966	0.936	0.755	0.771	0.760
Em90V					1.00	0.960	0.947	0.791	0.804	0.790
Em15H						1.00	0.959	0.761	0.783	0.780
Em25H							1.00	0.913	0.919	0.780
Em38H								1.00	0.919	0.932
Em60H									1.00	0.980
Em90H										1.00

Annexe 3: Paper Prigent et al., 2008.

A Parameterization of the Microwave Land Surface Emissivity Between 19 and 100 GHz, Anchored to Satellite-Derived Estimates

Catherine Prigent, Elodie Jaumouillé, Frédéric Chevallier, and Filipe Aires

Abstract—Land surface emissivities have been calculated for Tropical Rainfall Measuring Mission (TRMM) Microwave Instrument (TMI), Special Sensor Microwave/Imager (SSM/I), and Advanced Microwave Sounder Unit-A conditions, for two months (July 2002 and January 2003) over the globe at the European Centre for Medium-Range Weather Forecasts, directly from satellite observations. From this data set, a parameterization of the microwave emissivities that account for frequency, incidence angle, and polarization dependences is proposed. It is anchored to climatological monthly mean maps of the emissivities at 19, 37, and 85 GHz, which are calculated from SSM/I. For each location and time of the year, it provides realistic first-guess estimates of the microwave emissivities from 19 to 100 GHz, for all scanning conditions. The results are compared to radiative transfer model estimates. The new estimates provide rms errors that are usually within 0.02, with the noticeable exception of snow-covered regions where the high spatial and temporal variabilities of the emissivity signatures are difficult to capture.

Index Terms—Emissivity, land surface, microwave.

I. INTRODUCTION

FOR A large range of applications, there is a need for land surface microwave emissivity estimates, for all observation angles and polarizations, for the whole globe. Surface-sensitive microwave channels from satellite-borne instruments contain some key information about surface temperature, lower troposphere temperature, cloud liquid water, and precipitating water. Accurate microwave land surface emissivities are essential to properly extract such information in 1-D retrievals or within complex 4-D data assimilation systems in Numerical Weather Prediction (NWP) centers. The interaction between microwave radiation and the land surface is complex, being dependent on a large number of highly variable surface characteristics, such as soil humidity and roughness, vegetation properties, or snow cover. An extensive body of research has been directed toward a better understanding of the mechanisms

responsible for the microwave emission of land surfaces, from field experiments (using ground-based [1] or airborne sensors [2]), from radiative transfer modeling [3], [4], and from emissivity estimates derived from satellite observations [5]–[7].

Field experiments, which are under controlled conditions, provide high temporal and spatial resolution of the surface emissivity and make it possible to analyze the effect of detailed surface processes on the surface emissivity (e.g., freeze–thaw cycle, leaf orientation, or rain effect). However, they are performed for a limited number of surface types, observed under specific conditions (frequency and incidence angle), and have a difficulty in encompassing the large spatial and temporal variability of the surfaces measured from satellites at a global scale.

Land surface emissivity models have been developed for the globe for various surface conditions encountered over the continents [4], [8], using different radiative transfer solutions depending on the surface characteristics. Model inputs are provided by a land surface model, such as the one in the Global Data Assimilation System of the National Center for Environmental Prediction (NCEP) [4]. For specific surfaces and regional applications, coupling of land surface outputs with a radiative model can be efficient [9]. However, even when assuming that a perfect land surface emissivity model exists, the inputs it will require on a global basis (e.g., soil composition, texture, humidity, or roughness, vegetation and snow characteristics) would not be easily available with the spatial resolution compatible with the satellite and with the required accuracy.

Global land surface emissivity maps have been produced directly from satellite observations. For instance, emissivity atlases are calculated from Special Sensor Microwave/Imager (SSM/I) measurements [5], [7], by removing the contribution of the atmosphere, clouds, rain, and the surface temperature, using ancillary data. The emissivities are estimated for SSM/I observation conditions, i.e., between 19 and 85 GHz at 53° incidence angle, and for both vertical and horizontal polarizations. Advanced Microwave Sounder Unit (AMSU) emissivities have also been calculated [6], [10]. However, these satellite estimates are limited to the observation conditions of the given satellite (frequency, incidence angle, and polarization). For a given period of time, AMSU only provides a limited number of overpasses of the same location with the same incidence angle and does not give access to the vertical and horizontal polarization information separately. In addition, direct calculation of the emissivities from satellite observations requires a large amount of ancillary information that is not always easily accessible.

Good cloud filtering and a reliable surface skin temperature are particularly needed.

In order to provide the community with land surface emissivity estimates for the globe for all observing conditions (incidence angles and polarizations) between 19 and 100 GHz, we propose to derive a parameterization of the frequency, angular, and polarization dependences of the emissivity, anchored on a reliable satellite-derived emissivity database. First, satellite-derived estimates of the land surface emissivities are calculated from Tropical Rainfall Measuring Mission (TRMM) Microwave Instrument (TMI), SSM/I, and AMSU-A observations, for two months (July 2002 and January 2003) for the globe to analyze the frequency, angular, and polarization dependences for the different land surface types. A parameterization of the emissivity frequency, angular, and polarization dependences is deduced for each surface type. This parameterization along with the previously calculated SSM/I emissivity climatology at 19, 37, and 85 GHz for both polarizations at 53° provides an emissivity estimate for all locations on Earth for each month of the year, for all the incidence angles and polarizations between 19 and 100 GHz. The results are compared with model outputs.

II. EMISSIVITY DATA SETS

For a comprehensive analysis of the emissivity variations with surface type, frequency, angle, and polarization, this study examines and compares several sources of land surface microwave emissivity estimates, including satellite-derived values and model results.

A. Satellite-Derived Emissivity Data Sets

1) SSM/I, TMI, and AMSU-A Emissivity Database: In order to examine the frequency, angular, and polarization dependences for the full range of possible land surface conditions, microwave emissivities have been calculated at the European Centre for Medium Range Weather Forecasts (ECMWF) for all continents for two contrasted months (July 2002 and January 2003) from the satellite measurements derived from the following three instruments that have different observing conditions: SSM/I, TMI, and AMSU-A.

The Special Sensor Microwave/Imager (SSM/I) onboard the Defense Meteorological Satellite Program (DMSP) polar orbiters observes the Earth twice daily at 19.35, 22.235, 37.0, and 85.5 GHz with both the vertical and horizontal polarizations, with the exception of the 22 GHz (vertical polarization only). The observing incidence angle is close to 53°, and the fields of view decrease with frequency, from 43 × 69 km to 13 × 15 km [11].

The TMI is similar to SSM/I, with the addition of a lower frequency channel, a tropical orbit, and a better spatial resolution. It measures the microwave radiation in the tropical region from ∼40° S to ∼40° N, at five frequencies, 10.65, 19.35, 21.30, 37.00, 85.50 GHz, for both the vertical and horizontal polarizations (except at the 21.30 GHz which is only observed in the vertical polarization). The incidence angle is ∼53°. The spatial resolution ranges from 36.8 × 63.2 km at 10.65 GHz to 4.6 × 7.2 km at 85.50 GHz.

The AMSU-A onboard the NOAA polar orbiters provides atmospheric temperature profiling capabilities [12]. The window channels are at 23.8, 31.4, and 89 GHz. It is a cross-track scanning instrument, with 30 scan positions at 3.3° intervals from −14.5 × 3.3° to +14.5 × 3.3° which translate into local zenith angles θ_z up to 58.5°. The spatial resolution is 50 km at nadir. The polarization measured by AMSU-A rotates with the scan angle due to the rotating-reflector/fixed-feed type of antenna design and is a known mix of the vertical and horizontal polarizations (see [10] for more details).

The emissivity calculation method follows closely the scheme that was previously developed for SSM/I, which is described in detail in [5] and [7]. In this work, the selection of the clear pixels is based on the forecast model at ECMWF (not on the cloud flag from the International Satellite Cloud Climatology Project (ISCCP) [13] like in the previous work with SSM/I as this information is not available on real time to NWP centers). The observations that correspond to a nonzero fractional area cloud cover in the model are excluded. The atmospheric contribution is calculated from the ECMWF forecast model variables using the radiative transfer for the Tiros Operational Vertical Sounder (RTTOV) [14], [15].

An example of satellite-derived emissivity maps, which were calculated under clear-sky conditions and averaged over July 2002, is presented at 31.4 GHz from the AMSU-A observations for the incidence angles between 10° and 20° (Fig. 1). The holes in the maps correspond to the regions that are considered persistently cloudy during the month by the ECMWF forecast model.

2) Reference SSM/I-Derived Emissivity Database Over a Decade: The microwave land surface emissivities have been calculated over the globe for approximately ten years between 19 and 85 GHz at a 53° incidence angle for both vertical and horizontal polarizations using SSM/I observations. Ancillary data (ISCCP products [13] and NCEP reanalyses [16]) help remove the contribution from the atmosphere, clouds, and rain from the measured satellite signal and separate surface temperature from emissivity variations. This data set has been extensively evaluated (e.g., [7]), and in this study, it serves as a reference from which a monthly mean emissivity climatology is calculated and an emissivity-based surface-type classification is derived. This reference database is accessible at http://geo.obspm.fr/.

B. Model-Derived Emissivity Database

For comparison purposes, the emissivities have also been calculated at ECMWF, using the radiative transfer model from Weng *et al.* [4] with the forecast-model-relevant surface variables (soil temperature and humidity, vegetation fraction, and snow depth) as inputs. This model uses different solutions depending on the surface type.

III. ANALYSIS OF THE EMISSIVITY FREQUENCY AND ANGULAR DEPENDENCES

In order to facilitate the analysis of the frequency and angular dependences of the SSM/I, TMI, and AMSU emissivities, the data set is sorted per surface types. Instead of using an external
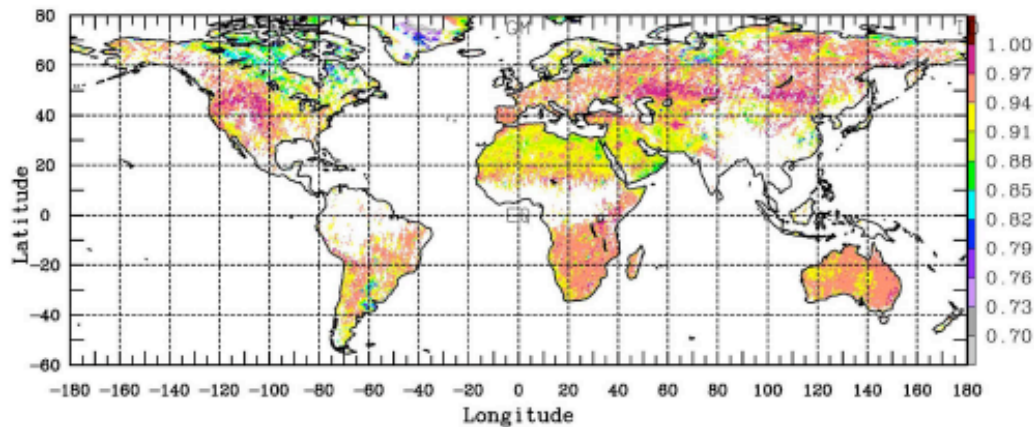
Fig. 1. Satellite-derived emissivity from AMSU-A at 31.4 GHz for July 2002 for the incidence angles between 10° and 20°.
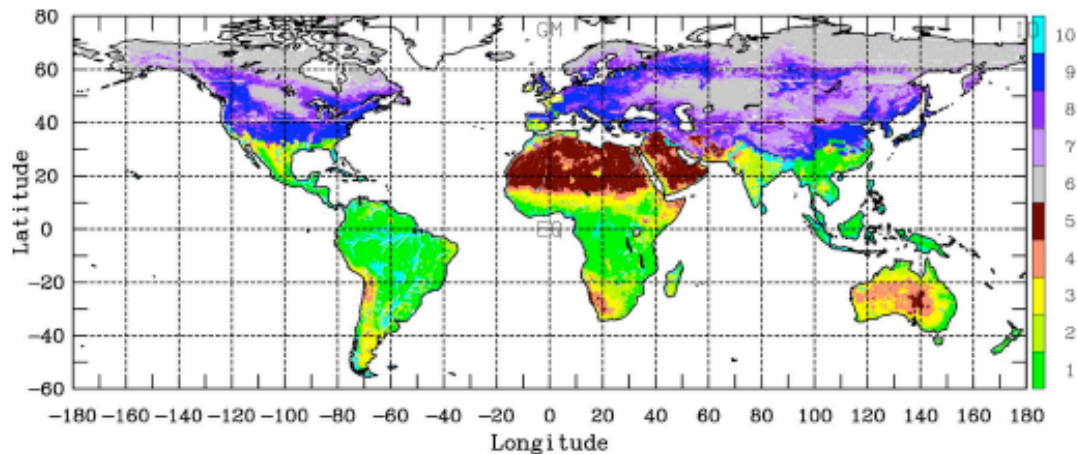

Fig. 2. Result of the classification of SSM/I derived emissivities for January. Classes from 1 to 5 represent continental snow-free regions. Classes 6 to 9 correspond to snow-covered land, and pixels with standing water are grouped in class 10.

and independent classification of vegetation, we develop a classification of the SSM/I emissivity, based on the reference SSM/I emissivity data set: this insures that each class represents a different behavior in terms of microwave emissivities and that the set of classes describes the full variability of these emissivities. The frequency and angular dependences of the satellite-derived emissivities are then analyzed for each surface type and compared to the model ones.

A. Classification of the Emissivity Data Set

The monthly mean emissivity climatology is calculated from the decadal (1992–2001) SSM/I emissivity database. An unsupervised clustering technique is applied to this emissivity climatology for the seven SSM/I channels. The chosen classification scheme (topological method from [17]) imposes a neighborhood requirement on nearby classes so that results are

easier to interpret (for more details on the classification method, see [18]). The clustering method is applied twice as follows: once for the snow-free pixels, then for the snow-covered pixel (the snow and ice information is extracted from the National Snow and Ice Data Center; ice pixels are not considered). Five classes are isolated for the snow-free regions, corresponding to vegetation densities, from dense vegetation (class 1) to desert surfaces (class 5), and four snow classes are also determined. Pixels with more than 10% standing water are not considered in the clustering scheme and are grouped in class 10: it includes areas of rivers or lakes, as well as regions associated with seasonal wetlands as defined by [19]. Fig. 2 shows the result of the classification for the month of January applied to the reference data set. The snow-free classes (from 1 to 5) show consistent spatial structures related to vegetation density. Note that given the small number of classes considered here and the limited sensitivity of the passive microwave observations
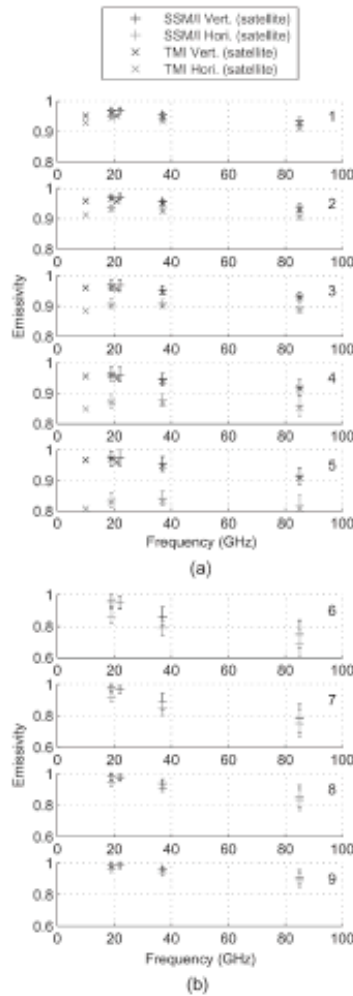
16

Fig. 3. Mean emissivity frequency dependence as observed from satellite-derived emissivities from the SSM/I and TMI at a 53° incidence angle, for both the vertical and horizontal polarizations for January 2003 (a) for the snow-free surface types and (b) for the snow-covered surfaces. The standard deviation is added for the SSM/I estimates.
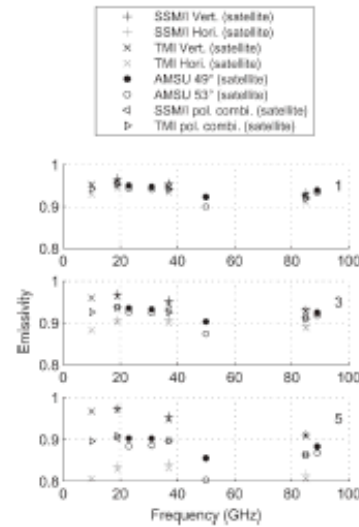

Fig. 4. Mean emissivity frequency dependence as observed from satellite-derived emissivities from the SSM/I, TMI, and AMSU-A around a 53° incidence angle for the three snow-free surface types. Both the vertical and horizontal polarizations are shown for the SSM/I and TMI. For AMSU-A, a polarization combination is measured, and for comparison, the same combination is calculated from the SSM/I and TMI perpendicular polarizations.

In the interpolation process, the emissivity of a specific location and month, for a given frequency, angle, and polarization, will be estimated from the actual emissivity of that location and month in the SSM/I-derived emissivity climatology, using the classification information only for the derivation of the frequency and angular dependences.

B. Frequency Dependence

1) Analysis With the Satellite-Derived Emissivities: The data set of two months of SSM/I, TMI, AMSU emissivities is sorted per surface types, using the SSM/I emissivity classification. For each snow-free class, Fig. 3(a) shows the frequency dependence of the SSM/I and TMI emissivity estimates in both polarizations, calculated from the satellite observations. The standard deviation over the class is indicated for the SSM/I estimates for each class. The results are shown for January 2003. The emissivities calculated from the satellite observations from SSM/I and TMI for the same frequencies agree very well for all the classes. The emissivities above 19 GHz have a very weak and close to linear frequency dependence, decreasing with frequencies, regardless of surface types. The TMI 21-GHz emissivity sticks out for all surface classes. It is likely related to an intercalibration problem. It could also be associated to a problem in the estimation of the absorption in the water vapor line, due to gaseous model errors or to errors in the water vapor profile estimates. This has not been elucidated. The 10-GHz emissivities are systematically and significantly lower than the 19-GHz ones, for both polarizations.

For the snow classes, Fig. 3(b) shows the frequency variation of the SSM/I emissivities (TMI does not cover the northern

at these frequencies to discriminate between very dense forest and moderate vegetation, most vegetated regions are grouped in classes 1 and 2. The snow classes as well present realistic structures, with class 6 related to dry and thick snow related to the strong scattering at 85 GHz, and class 9 associated to wet snow (see [20] for more details on the snow classification). We tried classifications with a higher number of classes, but this did not change significantly the final results of our analysis of the angular and frequency dependence of the emissivity. This basic classification was kept for this specific application. The same classification is then applied to the multisatellite two-month data set (SSM/I, TMI, and AMSU), based on the SSM/I emissivity values.
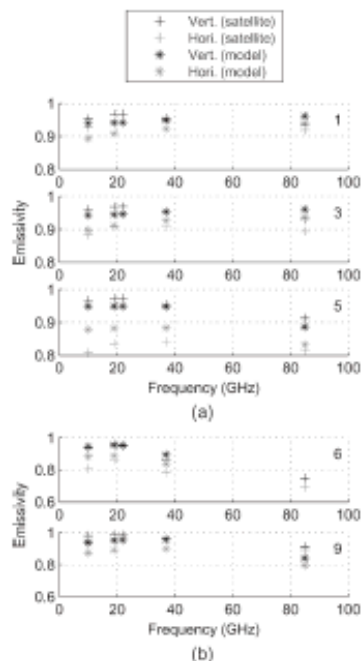
Fig. 5. Mean emissivity frequency dependence as observed from satellite-derived emissivities and from a model simulation at a 53° incidence angle, for both polarizations for January 2003, (a) for the snow-free surface types and (b) for the snow-covered surfaces. The satellite-derived estimates are from the SSM/I at 19 GHz and above and from TMI at 10 GHz. A limited number of classes are shown, the intermediate ones having an intermediate behavior. Note that the model values for the second snow type are out of the plotted range (lower values).

Fig. 6. Mean emissivity angular dependence as observed from satellite-derived emissivities from AMSU-A at 85 GHz, as compared to the SSM/I and TMI estimates at a 53° incidence angle in January 2003 (a) for three snow-free surface types and (b) for snow types.

latitudes and, as a consequence, provides very limited snow-emissivity estimates). The emissivity decreases with frequency. The slope is stronger for class 6 which corresponds to the very cold regions where snow grains are likely large and can significantly scatter the microwave radiation. The higher the frequency, the stronger the scattering, thus explaining the decrease of the emissivities with frequency [20].

Fig. 4 compares the AMSU emissivities derived from the satellite observations to the SSM/I and TMI satellite-derived emissivities. The AMSU satellite emissivities over 4° around 53° are averaged for comparisons with TMI and SSM/I. In addition to the vertical and horizontal polarizations, the polarization combination that corresponds to the AMSU geometry is added. The satellite emissivity estimate at 50.3 GHz is obviously problematic, which is likely contaminated by error in the atmospheric correction (see [10] for additional comments on this problem). At low frequencies, the SSM/I- and TMI-derived emissivities are larger than the AMSU ones. However, above 80 GHz, the opposite prevails regardless of the surface type.

2) Comparison With Model Estimates: Fig. 5 compares the SSM/I emissivity estimates from the satellite observations and from the Weng *et al.* model [4]. The satellite estimates show a much larger polarization dependence than the model over arid and low-density vegetations [classes 5 and 4 on Fig. 5(a)], par-
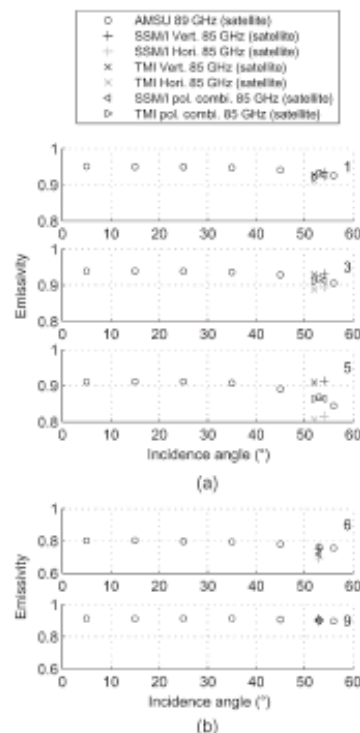
ticularly at low frequencies. The following two reasons could explain it: the model can overestimate the roughness effect, or the assumed surface parameters are not adequate. Regardless of the surface type, the satellite-derived emissivities decrease with increasing frequency. Over the arid regions (class 5), the emissivities predicted by the model are rather stable with frequencies up to 40 GHz, and then decrease. Over the vegetated regions (classes from 1 to 3), the modeled emissivities increase with frequencies for the horizontal polarization. At 10 GHz with TMI, large differences are observed between the satellite estimates and the model, particularly for the horizontal polarization and over the arid regions.

For snow-covered regions, the differences between the satellite and model emissivities are significant but the trends in the frequencies are similar (note that the scales on the y-axis on Fig. 5(a) and (b) are different and that the model values for the snow type 6 at 85 GHz are lower than the plotted range).

C. Angular Dependence

The analysis of the angular dependence of the satellite data can only be performed from the AMSU-A observations, i.e., not independently for each polarization.

The AMSU-satellite emissivities at 89 GHz are shown for different angles on Fig. 6, along with the SSM/I and TMI
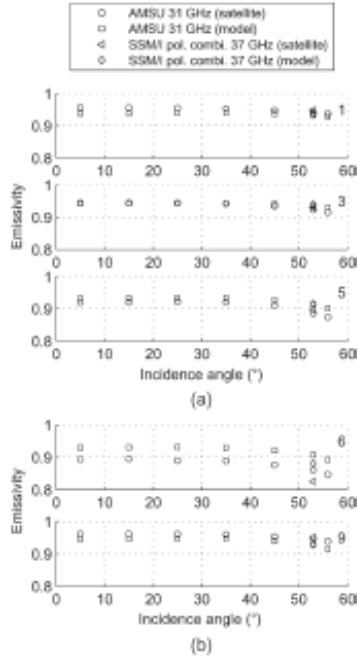
Fig. 7. Mean emissivity angular dependence as observed from satellite-derived emissivities from AMSU-A at 31 GHz and compared to the estimates at 37 GHz derived from SSM/I (a) for three snow-free surfaces and (b) for snow areas.
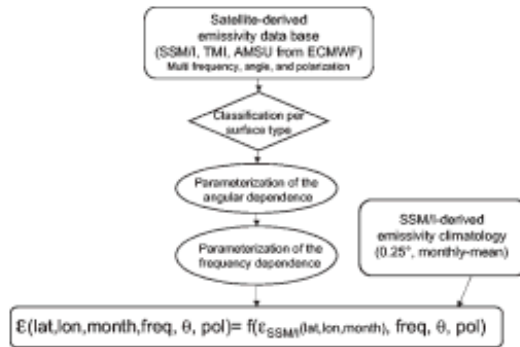

Fig. 8. Schematic presentation of the methodology.

satellite emissivities at 85 GHz. For all the surface types (snow-free and snow-covered regions), the angular dependence is smooth and limited: the polarization-combined AMSU emissivities are almost constant with the incidence angle up to 40° and then slightly decrease. The SSM/I- and TMI-derived emissivities around 53° at vertical and horizontal polarizations have been combined for comparison with the AMSU estimates. A rather good agreement is observed for all the surface types. Similar behaviors are seen at the other frequencies (not shown).

As compared to the model, the angular dependence of the satellite-derived emissivities is larger than the model ones
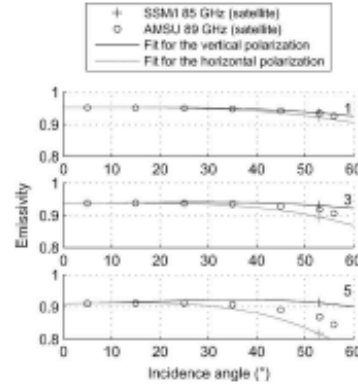

Fig. 9. Angular interpolation for each polarization, for three snow-free classes, as derived from the AMSU 89-GHz emissivities and anchored to the 85-GHz SSM/I emissivities.

(see Fig. 7 at 37 GHz; similar results are observed at the other frequencies). This is also related to the smaller polarization differences seen in the model than in the observation-derived emissivities.

IV. PARAMETERIZATION AND ITS RESULTS

Fig. 8 shows the methodology that is developed to derive the parameterization of the emissivity estimate for each location, month, frequency (between 19 and 100 GHz), incidence angle, and polarization. The development of the parameterization is based on the SSM/I and AMSU emissivity calculation performed at the ECMWF for January 2003, using only half the pixels for the snow-covered region. The method is then tested on the July 2002 emissivity calculations for the snow-free regions and on the remaining half of the January 2003 snow-covered pixels (as there is a very limited number of snow-covered pixels in July).

A. Parameterization of the Angular Dependence and Description of the Algorithm

1) Parameterization of the Angular Dependence: For each class that was previously defined, a polynomial function (third degree) is defined to describe the angular dependence of each polarization that fits both the SSM/I and AMSU-derived estimates. The polynomial function is calculated through a gradient descent to minimize the difference with the satellite-derived SSM/I and AMSU estimates. Fig. 9 shows the polynomial functions for three snow-free classes at 85 GHz, along with the corresponding satellite-derived emissivities from the SSM/I and AMSU.

2) Description of the Algorithm: The algorithm works as follows:

1) Selection of a location (latitude and longitude), month, frequency, and incidence angle. For a given location and month, a snow flag derived from the National Snow and Ice Data Center data is specified (snow or no snow).
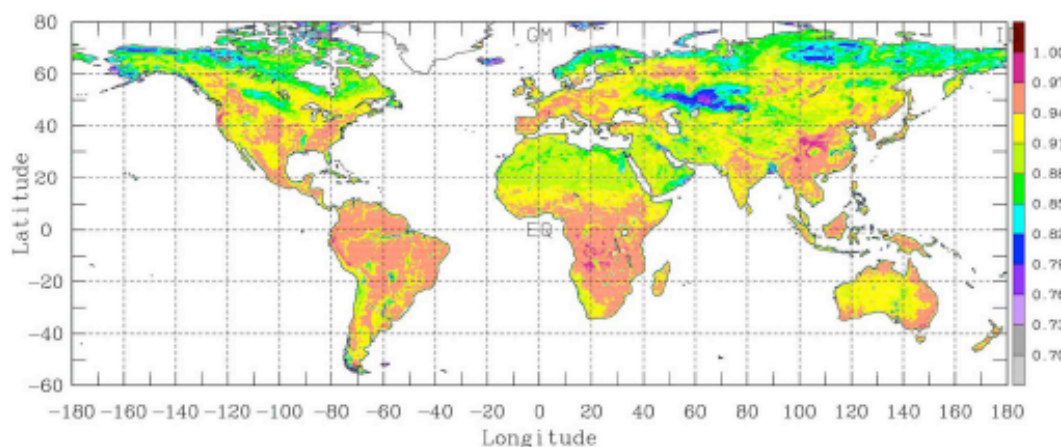
Fig. 10.   Example of an emissivity map at 30 GHz, for a 40° incidence angle, horizontal polarization in February.
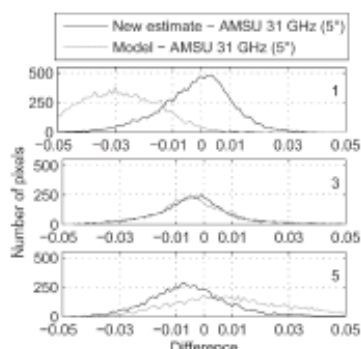

Fig. 11.   Histogram of the differences between the new interpolated emissivity and the satellite-derived emissivity, along with the difference between the modeled emissivity and the satellite-derived emissivity, at 31.4 GHz, 5° incidence angle, for AMSU-A for three snow-free classes.

2) Search in the SSM/I climatology database for the emissivities for that given location and month. It gives $e_v(53°)$ and $e_h(53°)$ for the SSM/I frequencies at 19.35, 37.0, and 85.5 GHz.

3) For each frequency (19.35, 37.0, and 85.5 GHz), calculation of the corresponding emissivity at nadir [$e_v(0°)$ and $e_h(0°)$] from a multilinear regression of $e_v(53°)$ and $e_h(53°)$. The coefficients of this multilinear regression have been calculated from each class, separately.

4) Application of the polynomial function that describes the angular dependence for each polarization and each SSM/I frequency to deduce the $e_v(\theta)$ and $e_h(\theta)$ emissivities.

5) Linear interpolation in frequency to derive $e_v(\theta)$ and $e_h(\theta)$ at the selected frequency from the three SSM/I frequency emissivity functions.

B. Results and Comparison With Other Estimates

Fig. 10 shows an example of parameterization at 30 GHz, at 40° incidence angle, horizontal polarization, for February.

The results of the parameterization are tested using the AMSU emissivities calculated at ECMWF for July 2002 and for half the pixels for January 2003 over snow. The ECMWF calculations are compared with both the parameterization results and the emissivity model outputs, which are also calculated at ECMWF (see Section II-B). The histograms of the differences for both estimates, at 31 GHz and 5° incidence angle, for the three snow-free classes are shown on Fig. 11. With the new parameterization over the snow-free regions, the differences are centered close to zero with a limited dispersion, regardless of the surface type. The behavior of the model is highly dependent on the surface type.

Table I summarizes the results of the comparison at 23, 31, and 89 GHz at 15° and 45° for each class. The bias is indicated, as well as the rms (in parentheses). Fig. 12 shows the rms error as a function of the surface class, for 15°, for both estimates.

For the snow-free regions, the new parameterization gives the rms values that are usually within 0.02, with a limited bias. Only a fraction of this error is directly related to the angular and frequency parameterization itself; the rest is due, first, to the temporal variabilities of the emissivities over a month and from year to year, and second, to the conditions of the calculation that were different at ECMWF and for the initial SSM/I emissivity climatology (Section II-A). The standard deviation of the emissivities within a month have been characterized [5] and are of the order of 0.01 at 19 GHz and can reach 0.02 at higher frequencies over snow (for the SSM/I emissivity database, these standard deviations are available along with monthly mean emissivities on our Web site geo.obspm.fr). The gaseous absorption model, the surface skin temperature, and the cloud detection schemes are different in the calculations performed at the ECMWF and for the initial SSM/I emissivity climatology, inducing potential differences between the calculated emissivities; the sensitivity of the calculation to these various factors have already been evaluated [5]. For classes 2 and 3, the rms errors of the model are also almost always below 0.03.

TABLE I
COMPARISON BETWEEN THE NEW PARAMETERIZATION AND THE SATELLITE-DERIVED EMISSIVITIES (A) AS WELL AS BETWEEN THE MODEL
ESTIMATES AND THE SATELLITE-DERIVED EMISSIVITIES (B) AT 23, 31, AND 89 GHz AT 15° AND 45° FOR EACH CLASS. THE BIAS IS
INDICATED, AS WELL AS THE RMS (BETWEEN PARENTHESES)

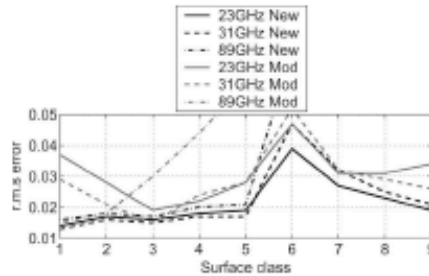| Class	15° 23GHz	45° 23GHz	15° 31GHz	45° 31GHz	15° 89GHz	45° 89GHz
1 (a)	-.003(.014)	.003(.015)	-.003(.013)	.001(.014)	.006(.016)	.006(.018)
1 (b)	-.034(.037)	-.028(.033)	-.025(.029)	-.020(.026)	.003(.015)	.009(.020)
2 (a)	-.006(.017)	.002(.018)	-.005(.016)	.000(.017)	.003(.018)	.005(.020)
2 (b)	-.024(.028)	-.017(.024)	-.016(.021)	-.010(.018)	.009(.018)	.017(.024)
3 (a)	-.003(.016)	.006(.018)	-.002(.015)	.004(.017)	.007(.017)	.010(.021)
3 (b)	-.010(.019)	-.002(.019)	-.002(.015)	.005(.019)	.020(.030)	.027(.037)
4 (a)	-.003(.018)	.007(.021)	-.002(.017)	.005(.020)	.009(.020)	.014(.027)
4 (b)	.003(.022)	.013(.029)	.010(.024)	.019(.031)	.017(.044)	.028(.054)
5 (a)	-.003(.019)	.012(.022)	-.003(.017)	.007(.019)	.010(.021)	.017(.030)
5 (b)	.009(.028)	.019(.032)	.012(.028)	.020(.032)	-.033(.060)	-.023(.062)
6 (a)	-.006(.039)	.008(.037)	.001(.047)	.010(.042)	.046(.070)	.051(.070)
6 (b)	.013(.047)	.024(.049)	.029(.052)	.040(.060)	-.309(.402)	-.308(.399)
7 (a)	-.005(.027)	.007(.029)	.009(.032)	.011(.033)	.036(.066)	.041(.068)
7 (b)	-.017(.031)	-.006(.028)	-.001(.032)	.008(.036)	-.327(.415)	-.328(.417)
8 (a)	-.001(.023)	.008(.027)	.003(.025)	.004(.030)	.005(.071)	.007(.071)
8 (b)	-.021(.031)	-.015(.029)	-.010(.029)	-.005(.031)	-.180(.300)	-.188(.309)
9 (a)	-.004(.019)	.003(.020)	-.003(.021)	-.000(.023)	-.004(.061)	.001(.062)
9 (b)	-.030(.034)	-.027(.032)	-.018(.026)	-.016(.025)	-.080(.166)	-.089(.179)

Fig. 12. RMS error between the new parameterization and the satellite-derived emissivities (black lines), as well as between the model estimates and the satellite-derived emissivities (gray lines) at 23, 31, and 89 GHz at 15° as a function of surface class.

For the snow-covered regions, much larger errors are observed, particularly at high frequencies for the snow classes that correspond to low emissivities (classes 6 and 7). In these regions, snow signatures are dominated by scattering, particularly at high frequencies, with a large temporal and spatial variability related to snow-grain metamorphism [20].

The emissivity model outputs have larger bias and rms for most cases. The ability of the model to represent the complexity of the radiation/surface interaction can be questioned. However, a large part of the error is likely related to the simplicity of the ECMWF surface model from which the emissivity model inputs are derived. This is particularly true over snow, where parameters like grain size distribution and stratification have a strong effect on the emissivity but are not available from the land surface models.

V. CONCLUSION

The angular and frequency dependences of the microwave land surface emissivities are analyzed between 10 and 90 GHz from estimates derived from SSM/I, TMI, and AMSU and are compared to model calculations. For a given surface type, both the angular and frequency dependences are rather limited and monotonic above 19 GHz. Below 19 GHz, the frequency dependence is different, and an additional work is to be performed, using Advanced Microwave Scanning Radiometer observations for instance. The general frequency and angular behaviors are rather similar, from models and satellite-derived emissivities, but differences in emissivities can be more than 10%.

From the analysis of the satellite-derived frequency and angular dependences, a parameterization is developed to estimate global microwave emissivities from the 19 to 100 GHz range for all the incidence angles and for both polarizations. It is anchored to a monthly mean emissivity climatology derived from the SSM/I observations for over a decade. The results are compared with model outputs and satellite estimates. The rms error is expected to be lower than 0.02 in snow-free region. The parameterization algorithm is available to the community, as well as the monthly mean emissivity climatology which it requires as inputs. The covariance of the emissivities from the original SSM/Iderived database is also accessible.

The uses of these emissivities are manifold as follows:

1) estimate the surface contribution in a cloud-clearing procedure;
2) as the first guess in the assimilation of close-to-the-surface sounding channels;
3) as the first guess in surface skin temperature retrievals using microwave observations for an "all-weather" estimate of the surface temperature to complement the infrared estimates that are only available under clear-sky condition;
4) evaluate the surface background contribution in precipitation and cloud retrievals;
5) simulate the responses of future instruments.

Efforts have to be conducted in collaboration with the land surface and emissivity modelers to better understand the differences observed between the satellite-derived and modeled emissivities. That will lead to the development of reliable and accurate emissivity models for global applications.

21

ACKNOWLEDGMENT

REFERENCES

[1] C. Matzler, "Passive microwave signatures of landscapes in winter," *Meteor. Atmos. Phys.*, vol. 54, no. 1–4, pp. 241–260, Mar. 1994.

[2] T. J. Hewison, "Airborne measurements of forest and agricultural land surface emissivity at millimeter wavelengths," *IEEE Trans. Geosci. Remote Sens.*, vol. 39, no. 2, pp. 393–399, Feb. 2001.

[3] J. Shi, K. S. Chen, Q. Li, T. J. Jackson, and P. E. O'Neil, "A parameterized surface reflectivity model and estimation of bare-surface soil moisture with L-band radiometer," *IEEE Trans. Geosci. Remote Sens.*, vol. 40, no. 12, pp. 2674–2686, Dec. 2002.

[4] F. Weng, B. Yan, and N. C. Grody, "A microwave land emissivity model," *J. Geophys. Res.*, vol. 106, no. D17, pp. 20 115–20 123, 2001.

[5] C. Prigent, W. B. Rossow, and E. Matthews, "Microwave land surface emissivities estimated from SSM/I observations," *J. Geophys. Res.*, vol. 102, no. D18, pp. 21 867–21 890, 1997.

[6] F. Karbou, C. Prigent, L. Eymard, and J. Pardo, "Microwave land emissivity calculations using AMSU measurements," *IEEE Trans. Geosci. Remote Sens.*, vol. 43, no. 5, pp. 948–959, May 2005.

[7] C. Prigent, F. Aires, and W. B. Rossow, "Land surface microwave emissivities over the globe for a decade," *Bull. Amer. Meteorol. Soc.*, vol. 87, no. 11, pp. 1573–1584, Nov. 2006. DOI:10.1175/BAMS-87-11-1573.

[8] T. Pellerin, J.-P. Wigneron, J.-C. Calvet, and P. Waldteufel, "Global soil moisture retrieval from a synthetic L-band brightness temperature data set," *J. Geophys. Res.*, vol. 108, no. D12, p. 4364, 2003. DOI:1.1029/2002JD003086.

[9] A. Wiesmann, C. Fierz, and C. Matzler, "Simulation of microwave emission from physically modeled snowpacks," *Ann. Glaciol.*, vol. 31, no. 1, pp. 397–405, Jan. 2000.

[10] C. Prigent, F. Chevallier, F. Karbou, P. Bauer, and G. Kelly, "AMSU—A land surface emissivity estimation for numerical weather prediction assimilation schemes," *J. Appl. Meteorol.*, vol. 44, no. 4, pp. 416–426, Apr. 2005.

[11] J. P. Hollinger, J. L. Pierce, and G. A. Poe, "SSM/I instrument evaluation," *IEEE Trans. Geosci. Remote Sens.*, vol. 28, no. 5, pp. 781–790, Sep. 1990.

[12] R. W. Saunders, "Note on the advanced microwave sounding unit," *Bull. Amer. Meteorol. Soc.*, vol. 74, pp. 2211–2212, 1993.

[13] W. B. Rossow and R. A. Schiffer, "Advances in understanding clouds from ISCCP," *Bull. Amer. Meteorol. Soc.*, vol. 80, no. 11, pp. 2261–2287, Nov. 1999.

[14] J. R. Eyre, "A fast radiative transfer model for satellite sounding systems," ECMWF, Reading, U.K., p. 1991, ECMWF Tech. Memo. 176.

[15] R. Saunders, M. Matricardi, and P. Brunel, "An improved fast radiative transfer model for assimilation of satellite radiance observations," *Q. J. R. Meteorol. Soc.*, vol. 125, no. 556, pp. 1407–1425, Apr. 1999.

[16] E. Kalnay *et al.*, "The NCEP/NCAR 40-year reanalysis project," *Bull. Amer. Meteorol. Soc.*, vol. 77, no. 3, pp. 437–470, Mar. 1996.

[17] T. Kohonen, *Self-Organization and Associative Memory*. New York: Springer-Verlag, 1984.

[18] C. Prigent, F. Aires, W. B. Rossow, and E. Matthews, "Joint characterization of vegetation by satellite observations from visible to microwave wavelength: A sensitivity analysis," *J. Geophys. Res.*, vol. 106, no. D18, pp. 20 665–20 685, 2001.

[19] C. Prigent, F. Papa, F. Aires, W. B. Rossow, and E. Matthews, "Global inundation dynamics inferred from multiple satellite observations, 1993–2000," *J. Geophys. Res.*, vol. 112, D12107, 2007.

[20] E. Cordisco, C. Prigent, and F. Aires, "Snow characterization at a global scale with passive microwave satellite observations," *J. Geophys. Res.*, vol. 111, no. D19, D19102, 2006. DOI:10.1029/2005JD006773.

Catherine Prigent received the Ph.D. degree in physics from Paris University, Paris, France, in 1988.

Since 1990, she has been a Researcher with the Laboratoire d'Etudes du Rayonnement et de la Matière en Astrophysique, Paris Observatory, Centre National de la Recherche Scientifique (CNRS), Paris, France. From 1995 to 2000, she was on leave from CNRS and worked at the NASA Goddard Institute for Space Studies, Columbia University, New York, NY. Her research interests focus on passive microwave remote sensing of the Earth. Her early work focused on the modeling of the sea surface emissivities at microwave wavelengths and the estimation of atmospheric parameters over the ocean from microwave measurements. Currently, her main interests include the calculation and analysis of microwave land surface emissivities, estimation of atmospheric and surface parameters over land from microwave observations, as well as multisatellite characterization of the land surface. She is also involved in satellite remote sensing of clouds with the analysis of passive-microwave observations over convective cloud structures.

Elodie Jaumouillé received the M.S. degree in applied mathematics from Bordeaux I University, Bordeaux, France, in 2005. She is currently working toward the Ph.D. degree in applied mathematics at Cemagref, Bordeaux.

She was with the Laboratoire des Sciences du Climat et de l'Environnement, Commissariat à l'Énergie Atomique, Gif-Sur-Yvette Cedex, France, where she was involved in the numerical and scientific validation of several climate models' outputs. Then, she is with the Laboratoire d'Etudes du Rayonnement et de la Matière en Astrophysique, Paris Observatory, Paris, France. She studied the frequency and angular variations of microwave emissivities. She is investigating how to control the hydraulic state of a drinkable-water network in order to minimize losses and to assure a better quality for the customer.

Frédéric Chevallier received the M.S. degree in physics at the University of Rennes, Rennes, France, in 1993. His Ph.D. work, which he defended in 1998, consisted of the development of a neural-network-based infrared radiation model for use in general circulation models. This study took place at the Laboratoire de Météorologie Dynamique, Palaiseau Cedex, France.

In 1998, he was with the European Centre for Medium Range Weather Forecasts, Reading, U.K., to work in the physical aspects and satellite sections. There he adapted his radiation model, which was made operational in 2003 as part of the 4-D-Var physics. His involvement in the data assimilation system increased over the years, particularly in initiating the assimilation of cloud-affected and rain-affected satellite radiances. He was appointed as a Permanent Research Scientist with the Laboratoire des Sciences du Climat et de l'Environnement, Gif-Sur-Yvette Cedex, France, in December 2003. His current research interests focus on the Bayesian inversion of the surface fluxes of atmospheric compounds from *in situ* and remote sensing atmospheric measurements.

Filipe Aires received the Ph.D. degree in statistics from the University Paris–Dauphine, Paris, France, in 1999.

He was with the NASA Goddard Institute for Space Studies, New York, NY, for five years, and he is now a Research Scientist with the Laboratoire de Météorologie Dynamique, Centre National de la Recherche Scientifique, Palaiseau Cedex, France. His research interests focus on satellite remote sensing of the Earth and statistical analysis of the climate. In earlier works, he analyzed climatic signals, using statistical techniques such as independent component analysis. He has also defined new tools for the characterization of climate feedback. He has developed multiinstrument and multiparameter remote sensing algorithms to retrieve atmospheric variables such as temperature, ozone, or water vapor profiles, and surface variables such as surface skin temperature, vegetation indices, or microwave emissivities. Instruments involved in these remote sensing studies include Advanced Microwave Sounder Unit, Special Sensor Microwave/Imager, Infrared Atmospheric Sounding Interferometer, European Remote-Sensing, and TIROS Operational Vertical Sounder. Currently, he is involved in the development of remote sensing algorithms for the French–Indian mission Megha-Tropiques.

22

Annexe 4: Paper Aires et al. 2009 (Preprint)

A Tool to Estimate Land Surface Emissivities at Microwaves frequencies (TELSEM) for use in numerical weather prediction.

Filipe Aires[*1], Catherine Prigent[2], Frédéric Bernardo[3], Carlos Jiménez[2], Roger Saunders[4], Pascal Brunel[5]

[1]*Laboratoire de Météorologie Dynamique / IPSL / CNRS, Université de Paris VI/Jussieu, France*

also Associate at Laboratoire de l'Etude du Rayonnement et de la Matière en Astrophysique, CNRS, Observatoire de Paris, France

[2]*Laboratoire de l'Etude du Rayonnement et de la Matière en Astrophysique, CNRS, Observatoire de Paris, France*

[3]*Laboratoire de Météorologie Dynamique / IPSL / CNRS, Université de Paris VI/Jussieu, France*

[4]*MetOffice, Exeter, England*

[5]*Météo-France Lannion, France*

Abstract: A Tool to Estimate Land Surface Emissivities at Microwaves (TELSEM) frequencies has been developed, for use with the Radiative Transfer TOV (RTTOV) model. Its objective is to facilitate the retrieval of atmospheric profiles over land, from satellite microwave sounders, especially the assimilation of radiances in Numerical Weather Prediction (NWP) models. TELSEM provides emissivity estimates and error covariance matrices for all land surfaces, between 19 and 100 GHz, and for all angles and linear polarizations. It is anchored to a pre-calculated monthly mean emissivity climatology derived from Special Sensor Microwave/ Imager (SSM/I) observations. Tests show that it can be applied with benefits down to 5 GHz and up to 190 GHz, for atmospheric profile retrievals over land. Copyright © 2009 Royal Meteorological Society

KEY WORDS   class file; LaTeX 2_ε; *Q. J. R. Meteorol. Soc.*

1 Introduction

Surface-sensitive microwave observations from satellite instruments contain key information about lower-troposphere temperature and water vapour, cloud liquid water and precipitating water. Accurate estimates of microwave land surface emissivities are essential to extract such information in any inversion scheme such as 1D retrievals or within complex 4D data assimilation

[*]Correspondence to: F. Aires, CNRS/IPSL/Laboratoire de Meteorologie Dynamique, Université Pierre et Marie Curie, case 99, 4, place Jussieu, F-75252 PARIS Cédex 05, France (filipe.aires@lmd.jussieu.fr)

[†]Please ensure that you use the most up to date class file, available from the QJRMS Home Page at

http://www.interscience.wiley.com/qj

systems in Numerical Weather Prediction (NWP) centers. However, surface-sensitive microwave observations are so far essentially only used over ocean. Over land, the surface emissivity is difficult to obtain: it is usually high, limiting the contrast with the atmospheric contribution, and very complex to model, being spatially very variable and dependant upon a large number of parameters (e.g., soil moisture, vegetation, snow cover).

Land surface emissivity models have been developed for the globe for various surface conditions (Weng et al., 2001; Pellerin et al., 2003), but they require a large number of input parameters that are not easily available such as soil composition, soil moisture, vegetation and snow characteristics. In parallel, global land surface emissivity datasets have been produced, directly from satellite observations (Prigent et al., 1997). Microwave land surface emissivity have been calculated, from Special Sensor Microwave/Imager (SSM/I) measurements (Prigent et al., 1997, 2006) or from the Advanced Microwave Sounding Units (AMSU) (Prigent et al., 2005 a; Karbou et al., 2005), under clear-sky condition, by subtracting the atmospheric effect with the help of ancillary data. This approach is difficult to implement directly in an atmospheric retrieval scheme: it requires a cloud clearing procedure, it can be computationaly demanding, and the emissivity estimates might not be robust for all types of configurations.

In order to perform satellite retrievals over land, another strategy can be used: Pre-computed emissivity atlases can provide an emissivity first guess that is adjusted in the inversion or assimilation scheme. However, this first-guess needs to be as close as possible to the real emissivities, in particular taking into account the angle, frequency and polarization dependencies. In a previous work (Prigent et al., 2008), a parameterization of the land surface emissivities between 19 and 100 GHz

under all observing conditions has been derived, based on an analysis of the frequency, angular, and polarization dependencies of the emissivities calculated from SSM/I, Tropical Rainfall Measuring Mission (TRMM) Microwave Instrument (TMI), and AMSU. The RMS errors for these parameterized emissivities have been estimated to be lower than 0.02 in snow-free regions.

This paper reports on a Tool to Estimate Land Surface Emissivities in the Microwaves (TELSEM), developed within the Radiative Transfer TOV (RTTOV) model (Saunders et al., 1999), to provide microwave radiance users (in particular the NWP community) with robust first guess of emissivity estimates. This emissivity calculator also provides realistic estimates of the errors, including the covariance matrix. In Section 2, the emissivity interpolation method is summarized and the emissivity calculation tool is described. Applications of this tool are presented in Section 3.

Note that this microwave emissivity tool is generic and flexible: it can be interfaced with other radiative code such as the Community Radiative Transfer Model (CRTM) developed by the Joint Center for Satellite Data Assimilation (JCSDA) (Weng and Liu, 2003).

2 The land surface emissivity estimates, its associated errors, and its implementation in the radiative transfer code

2.1 The emissivity parameterization

Monthly-mean emissivity atlases have been produced and analyzed, for the 1993-2004 period, from SSM/I measurements (Prigent et al., 2006), by removing the contribution

of the atmosphere, clouds, rain, and the surface temperature, using ancillary data and radiative transfer calculations. The reference SSM/I-derived land surface emissivity climatology is derived from these atlases. The emissivities are estimated for SSM/I observation conditions, i.e., between 19 and 85 GHz, at 53° incidence angle, and for both vertical and horizontal polarizations. These emissivities have been thoroughly analyzed. They provide key information on the surface characteristics and have been used in numerous applications (e.g., Prigent et al., 2001; 2007; Aires et al., 2005; Jimenez et al., 2009). Emissivities have also been estimated from AMSU measurements (Prigent et al., 2005 a; Karbou et al., 2005). These SSM/I and AMSU satellite estimates are limited to the observation conditions of the given satellite (frequency, incidence angle, and polarization). For instance, for a given period of time, AMSU only provides a limited number of overpasses of the same location with the same incidence angle, and does not give access to the vertical and horizontal polarization information separately. In order to derive general estimates of the emissivities, land surface emissivities calculated at European Centre for Medium-range Weather Forecasts (ECMWF) under a large range of frequencies, incidence angles, and polarizations have been analyzed from SSM/I, TMI, and AMSU-A observations, for two months (July 2002 and January 2003) over the globe.

SSM/I observes at 19.35, 22.235, 37.0, and 85.5 GHz with both vertical and horizontal polarizations, with the exception of 22 GHz (vertical polarization only). It is a conical scanner with incidence angle close to 53°. TMI frequencies are similar to the SSM/I ones, with the addition of a lower frequency channel (10.65 GHz), for both polarizations. In addition to the O_2 sounding channels around 55 GHz, AMSU-A has window channels at 23.8, 31.4, 50.2, and 89 GHz. It is a cross-track scanning instrument, with 30 scan positions up to 58.5°. The polarization rotates with scan angle due to the rotating-reflector/fixed-feed type of antenna design and is a known mix of the vertical and horizontal polarizations. The emissivity calculation method follows closely the scheme previously developed for SSM/I (Prigent et al., 2006). In the calculations performed at ECMWF, the selection of the clear pixels is based on the ECMWF forecast model and the atmospheric contribution is also calculated from the ECMWF forecast model variables using RTTOV.

In order to facilitate the analysis of the frequency and angular dependences of the SSM/I, TMI, and AMSU emissivities, the data set is sorted per surface types, using a classification of the SSM/I emissivity themselves, based on the reference SSM/I emissivity dataset: this ensures that each class represents a different behavior in terms of microwave emissivities and that the set of classes describes the full variability of these emissivities. The frequency and angular dependencies of the satellite-derived emissivities are then analyzed for each surface type and compared to the model ones. Five surface types are identified for snow-free regions, from dense forest to deserts, and four snow types are isolated. The 10th class indicates pixels that contain standing water. The analysis of this dataset showed that the frequency, angular and polarization dependences are related to surface types but can be parameterized rather simply, with the SSM/I-derived monthly-mean emissivity climatology as a basis for the parameterization. For each surface type, the angular and frequency dependences are smooth enough to describe the dependences with simple polynomial functions, anchored to the SSM/I emissivity climatology. For the location (latitude and longitude) and month selected by the user, the algorithm searches the corresponding SSM/I emissivity in the climatology database. It gives emisV(53°) and

emisH(53°), i.e. the Vertical and Horizontal polarization emissivity at 53° incidence angle, for the SSM/I frequencies at 19.35, 37.0 and 85.5 GHz. Then for each SSM/I frequency (19.35, 37.0, 85.5 GHz), the algorithm calculates the corresponding emissivity at nadir emisV(0°) (which equals emisH(0°)) from a multi-linear regression of emisV(53°) and emisH(53°). The coefficients of this multi-linear regression have been pre-calculated for each class, separately. The next step consists in applying the polynomial function that describes the angular dependence for each polarization and each SSM/I frequency to deduce the emissivities emisV(θ°) and emisH(θ°) at the incidence angle θ selected by the user. Finally, a linear interpolation in frequency is applied to derive emisV(θ°) and emisH(θ°) at the user's selected frequency, from the three SSM/I frequency emissivity functions. It should be mentioned that a climatology has been used to define in the emissivity atlas the location of snow-covered pixels. It is expected that the use of this climatology will bring problems during the snow melt/freezing because for a particular data, the reality of the situation can be different from the climatology.

For frequencies lower than 19 GHz, the 19 GHz emissivities are adopted. This will be evaluated down to 6 GHz in section 3. For frequencies higher than 85 GHz, the 85 GHz emissivities are used. AMSU-B emissivities at 150 GHz have been calculated directly from the satellite observations as described above. However, these calculations showed large variability related to water vapour errors and cloud contaminations, and tests proved that the use of the 85 GHz emissivity estimates were more reliable (Karbou et al., 2005).

Figure 1 shows an example of emissivity interpolation, for September at 31.4 GHz, for 15° incidence angle, vertical polarization. The interpolation scheme preserves the spatial structure of the microwave emissivities, for instance the hydrological features in South America or the geologicaly-related information in the North African desert (Prigent et al., 2005 b). More details on the parameterization and its evaluation are provided in Prigent et al. (2008).

2.2 Estimation of the error covariance matrices of the interpolated emissivities

For most applications, the errors associated to the emissivities have to be evaluated as this information is essential for most retrieval scheme, especially in assimilation systems. When emissivities under several conditions (at different frequencies or polarizations for instance) are used together, the covariance matrix of these errors also needs to be estimated.

An error budget has been estimated for the reference SSM/I-derived emissivities taking into account the various sources of errors in the calculation (Prigent et al., 1997): the accuracy of the instantaneous retrieved emissivities is estimated to be within 1%-2%. At monthly-mean scales, the standard deviation of the emissivity calculation for each frequency is considered as a measure of the error. Careful analysis and comparisons with other emissivity products validated this approach.

Let $Em_{SSMI}(6)$ be the 6-channels SSM/I emissivities from the reference climatology for the 19V, 19H, 37V, 37H, 85V, and 85H channels. The SSM/I emissivity climatology provides also the 6×6 correlation matrix, $Cor_{SSMI}(6, 6)$, for the uncertainties on the 6 SSM/I channels together with the associated vector of uncertainty standard deviation, $Std_{SSMI}(6)$. The covariance matrix of the SSM/I emissivity uncertainties can easily be estimated using:

$$Cov_{SSMI} = Std'_{SSMI} \cdot Cor_{SSMI} \cdot Std_{SSMI} \quad (1)$$

where $'$ denotes the transpose of the matrix. A study has been conducted to measure the variability of the correlation of errors for all the pixels in a particular surface type. It appeared (not shown) that the matrices Cor_{SSMI} were quite robust: For a particular surface type, the standard deviation of the correlations are small compared to the actual correlation. This means that, for each of the 10 surface types, a unique error correlation matrix Cor_{SSMI} can be estimated and then used. An example of such correlation matrix is given in Table I for class 1 (i.e., highly vegetated areas). The structure of this matrix is complex for each vegetation class and it varies from one class to another. The correlations between channels are highly significant and cannot be neglected. In particular, it is important to use this correlation structure in a variational assimilation experiment, and in all inversion schemes in general. If the covariance error matrix is assumed diagonal (i.e., only the standard-deviation of errors are accounted for), the uncertainties are under-estimated. The fact that a single correlation matrix is used for all the situations for a given surface type is a simplification that allows for a faster use of the interpolator, without any significant loss of accuracy. It is important to note that the Cor_{SSMI} correlation matrix is constant for each surface type, but the Std_{SMI} standard deviation matrix in the SSM/I emissivity climatology is provided by the interpolator so that each spatial location over land will have a different Cov_{SSMI} covariance matrix (Eq. (1)).

The goal of the emissivity interpolator is to estimate new emissivities $Em_{NEW}(f)$, where f is the number of new frequencies to be calculated by the interpolator (at different scanning angles and polarizations). The first half of Em_{NEW} is for the vertical polarizations and the second half for the horizontal ones (this is the way it has been implemented in the TELSEM code). The emissivity parameterization described in section 2.1 allows for the estimation of $Em_{NEW}(f)$ using a $(f \times 6)$-matrix, A, such that:

$$(Em_V; Em_H) = A \cdot Em_{SSMI} \quad (2)$$

The difficulty is then to have a realistic assessment of the errors of the interpolated emissivities. Simple algebra shows that the covariance matrix of the new emissivity uncertainties can be estimated by:

$$Cov_{NEW} = A' \cdot Cov_{SSMI} \cdot A$$

$$= A' \cdot Std'_{SSMI} \cdot Cor_{SSMI} \cdot Std_{SSMI} \cdot A \quad (3)$$

As a consequence, TELSEM not only provides a set of emissivities at new frequencies, angle and polarization, it also estimates the full covariance matrix on this new set of channels.

In summary, the standard deviation matrix Std_{SSMI} and the corresponding correlation matrix Cor_{SSMI} are provided by the reference emissivity climatology. The interpolator calculates the new covariance matrix Cov_{NEW} for each location over land, and for each month, for the frequencies specified by the user. Figure 2 provides the uncertainty estimates interpolated at 31.4 GHz, for the vertical polarization at 15° incidence angle, for September. As expected, large uncertainties are related to temporally variables features such as wetlands (e.g., over Bangladesh) or snow- or ice-covered regions (e.g., over Greenland).

2.3 Implementation of the emissivity module in the RTTOV code

The RTTOV model has been developed for very rapid calculations of radiances in the infrared and microwaves, primarily for use in variational assimilation of satellite observations within NWP centres (Saunders et al., 1999). It is jointly developed by the Met Office (UK), Météo-France, and ECMWF in the framework of the EUMETSAT-funded NWP Satellite Application Facility and also other EUMETSAT sponsored activities. The original code was described by Eyre and Woolf (1988). Matricardi et al. (2004) present more recent developments. It is a compromise between calculation accuracy and speed. The absorption models are parameterized to produce regressions as a function of a selection of model predictors such as temperature and humidity, based on training datasets of accurate line-by-line absorption models and representative atmospheric profiles aspects. RTTOV-9 has been released in 2008. RTTOV computes sea surface emissivity as a function of surface wind speed, using the FASTEM-3 code developed by Deblonde and English (2001)[†]. However, it does not provide accurate estimates of the land surface emissivity: a fixed microwave surface emissivity value (0.85) is suggested, regardless of the frequency and observing conditions (the impact of such a simplification will be measured in section 3 and in Figs. 4 and 5).

The TELSEM parameterization has been added as a new tool to the RTTOV simulator. The only information to be provided by the user is the geographical location (latitude and longitude) and the month. The nominal spatial resolution of the emissivity estimates is $0.25° \times 0.25°$ but, if desired, the user can specify another spatial resolution (always larger or equal to the initial one): the code will use

the closest climatology-derived emissivity or it will perform the spatial integration. Calculation can be performed individually for single frequency channels but also for multiple channels in which case error covariance matrices are provided. Figure 3 describes the different steps in the process.

3 Validation of the emissivity estimates

3.1 Comparison with observations for instruments on board the AQUA and MetOp platforms

In order to evaluate the new emissivities, RTTOV radiative transfer simulations with and without the new tool have been simulated and compared to satellite observations. Two experiments are performed, the first one with the observations from the Advanced Microwave Sounding Radiometer-E (AMSR-E) and the Humidity Sounder for Brazil (HSB) on board the Aqua satellite, and the second one with the AMSU-A and Microwave Humidity Sounder (MHS) on board the MetOp platform.

For the first experiment, AMSR-E and HSB observations are collected for July 2002 and January 2003. The observations from AMSR-E (conical scanning instrument) and from HSB (cross-track sounder) are colocated using a maximum time difference of less than 60 s and using for each AMSR-E pixel the closest HSB pixel. The atmospheric profiles and the surface temperature are extracted from the ECMWF analysis. Figure 4 (upper part) compares the simulated and observed brightness temperatures (TBs) over land, when using TELSEM in RTTOV and when using the emissivities computed by RTTOV itself, for clear (left) and cloudy (right) cases. Precipitating cases are excluded. For comparison purposes, the simulations have been performed over ocean as well (bottom), with the emissivities calculated with the

---

[†] See http://www.metoffice.com/research/interproj/ nwpsaf/rtm/rttov8_svr.pdf

FASTEM model (Deblonde and English, 2001). All incidence angles are included in these statistics.

The results are clearly better with the new land surface emissivity model, especially for the H polarization, with a RMS error divided by 3 in the window channels for this polarization (Figure 4 top left and right). The emissivities for the V polarization are usually high, often close to the 0.85 value adopted by the initial version of RTTOV, and as a consequence the differences between the new model and the former estimate are not significant. With the new land surface emissivity values, the results are similarly good for clear and cloudy scenes. As expected, there is no impact of the emissivity changes for opaque channels around 183 GHz. There is a positive impact, even at frequencies below 19 GHz, although the algorithm is not optimized for these frequencies. Above 19 GHz, the agreement between simulations and observations obtained with the new land surface emissivities is similar to the one obtained over ocean. At 85 GHz, it is even better. Note that the fact that the RMS error for cloudy case over ocean is larger than over land is likely not due to emissivity problems, but to the higher sensitivity to the clouds over ocean. At 150 GHz, the 85 GHz emissivity is adopted: the effect is not large but still positive. At this frequency and higher, the RMS error between the simulations and the observations is driven by the atmospheric components, with very similar behaviour over land and ocean, for both clear and cloudy situations. At frequencies above 100 GHz, for cloudy cases, the RMS error increases with frequencies, regardless of the emissivity, likely due to the increasing effect of scattering by clouds. No bias correction procedure[‡] was used for these comparison statistics, explaining part of the remaining differences.

[‡]The use of real observations in a remote sensing code requires most of the time some bias tuning of the data so that the RTM simulations are close enough to the real observations.

A similar experiment has been conducted with the MetOp microwave instruments, AMSU-A and MHS. The results are presented on Figure 5. The statistics are given for July 2007 and January 2008 observations. All incidence angles are used. Similar conclusions can be drawn: the use of the new emissivity interpolator improves the comparison. It can be noted in this figure that the land and ocean statistics are similar, even for the channels that are sensitive to the surface. This means that the introduction of realistic microwave emissivities has increased the accuracy of the simulations, which should improve the water vapor retrieval in the lower atmosphere over land.

3.2 Impact of the land surface emissivity in the inversion of atmospheric profiles

A French-Indian satellite mission, Megha-Tropiques will be launched in 2010 (Desbois et al, 2007). Its objective is to study the water cycle in the Tropics, with a high temporal sampling. Megha-Tropiques will carry two microwave instruments, a conical imager Madras with frequencies at 19, 23, 37, 89 and 157 GHz for both linear polarizations, and a cross-track humidity sounder Saphir with 6 channels around the 183 GHz water vapor line. A neural network inversion has been developed to derive, among other variables, the water vapor atmospheric profiles from the combination of the Madras and Saphir observations. The statistical method is trained on a simulated database using a global collection of ECMWF analysis coupled to the RTTOV radiative transfer model. The operational inversion algorithm uses the new RTTOV tool to estimate the emissivities over land.

In order to evaluate the operational chain, tests have been conducted on existing satellite data at similar frequencies, using AMSR-E and HSB observations from AQUA, over the Tropics ($\pm30°$) for two months (July 2002 and January 2003). Figure 6 shows the RMS errors

for the retrieval of the relative humidity, calculated from the difference between the satellite retrieval and the analysis from ECMWF, assuming that the ECMWF analysis is the truth. For both clear and cloudy atmospheres, the results show that the retrieval accuracies for the lower layers below 750 hPa are of the same order (around 10% in RMS) over land and ocean. This is very encouraging. So far, observations from surface-sensitive channels over land were disregarded. Our results suggest that the use of realistic emissivity estimates can considerably increase the number of satellite observations to be assimilated over land, and provide estimates of atmospheric profiles in the lower layers over land with accuracies that are comparable to the accuracies over the oceans.

4 Conclusion

A Tool to Estimate Land Surface Emissivities in the Microwaves (TELSEM) has been developed, within the RTTOV radiative transfer model, for a simple and convenient use by a large community. It is anchored to a climatological atlas of emissivities calculated from SSM/I. TELSEM is able to do interpolation in frequencies and viewving angle. It is originally designed for frequencies between 19 and 85 GHz but tests proved that it is beneficial down to 5 GHz and up to 190 GHz. TELSEM also provides the full covariance matrix of the uncertainties on the interpolated emissivities, a key information for most retrieval algorithms, especially for assimilation in NWP schemes.

The potential benefits of TELSEM for the inversion of surface-sensitive microwave sounding channels are illustrated by two examples. First, the emissivity interpolator has been used within the RTTOV model to simulate Aqua (AMSR-E/HSB) and MetOp (AMSU-A/MHS)

observations that have been compared to the corresponding real observations. Adding the land surface emissivity information has a strong positive impact, with a decrease of the bias of more than 10 K for some channels, averaged over two months at a continental scale. The benefit is larger for the horizontaly polarized channels. Using these realistic land surface emissivity estimates, the agreements between simulations and observations are similar over land and ocean, making it possible to attempt assimilation of surface-sensitive observations over the continents. A water vapor atmospheric retrieval experiement has been conducted, from combined AMSR-E and HSB data, using an adaptation of the operational chain developed for the future Megha-Tropiques mission. The ability to reproduce the observed TBs over land directly benefits the retrieval of the lower atmospheric layer, with retrieval accuracy comparable over land and ocean. TELSEM in RTTOV will be soon tested in an assimilation scheme in a NWP center.

References

Aires, F., C. Prigent, and W. B. Rossow, Sensitivity of microwave and infrared satellite observations to soil moisture at a global scale. II: Global statistical relationships, J. Geophys. Res., 110, D11103, doi:10.1029/2004JD005094, 2005.

Aires, F., M. Paul, C. Prigent, B. Rommen, and M. Bouvet, Measure and exploitation of multi-sensor and multi-wavelength synergy for remote sensing: an application for the retrieval of atmospheric temperature and water vapour from METOP, submited to J. Geophys. Res., 2009.

Deblonde, G. and S. J. English, Evaluation of the FASTEM-2 fast microwave oceanic surface emissivity model, Tech. Proc. ITSC-XI Budapest, 20-26 Sept 2000, 67-78, 2001.

Desbois, M., M. Capderou, L. Eymard, R. Roca, N. Viltard, M. Violier, N. Karouche, Megha-Tropiques : un satellite hydromtorologique franco-indien, La Météorologie, pp. 19-27, 2007

Eyre, J. R. and H. M. Woolf, Transmittance of atmospheric gases in the microwave region: a fast model, Appl. Optics, 27 3244–3249, 1988.

Jimenez, C., C. Prigent, and F. Aires, Toward an estimation of global land surface heat fluxes from multisatellite observations, J. Geophys. Res., 114, D06305, doi:10.1029/2008JD011392, 2009.

Karbou, F., C. Prigent, L. Eymard, and J. Pardo, Microwave land emissivity calculations using AMSU measurements, IEEE Trans. Geo. Remote Sens., 43, 948- 959, 2005.

Matricardi, M., F. Chevallier, G.A. Kelly, and J.-N. Thpaut, An improved general fast radiative transfer model for the assimilation of radiance observations, Quart. J. Roy. Meteorol. Soc., 130, 153-173, 2004.

Pellerin, T., J.-P. Wigneron, J.-C. Calvet, and P. Waldteufel, Global soil moisture retrieval from a synthetic L-band brightness temperature data set, J. Geophys. Res., 108, 4364, doi:1.1029/2002JD003086, 2003.

Prigent, W. B. Rossow, and E. Matthews, Microwave land surface emissivities estimated from SSM/I observations, J. Geophys. Res., 102, 867-21,890, 1997.

Prigent, F. Aires, W. B. Rossow, and E. Matthews, Joint characterization of vegetation by satellite observations from visible to microwave wavelength: A sensitivity analysis, J. Geophys. Res., 106, 20665-20685, 2001.

Prigent, C., F. Chevallier, F. Karbou, P. Bauer and G. Kelly, AMSU-A land surface emissivity estimation for numerical weather prediction assimilation schemes, J. Appl. Meteorol., 44, 416-426, 2005 a.

Prigent, C., J. Munier, B. Thomas, and G. Ruffi/'e, Microwave signatures over carbonate sedimentary platforms in arid areas: Potential geological applications of passive microwave observations?, Geophys. Res. Let., 32, L23405, doi:10.1029/2005GL024691, 2005 b.

Prigent, C., F. Aires, and W. B. Rossow, Land surface microwave emissivities over the globe for a decade, Bull. Amer. Meteorol. Soc., doi:10.1175/BAMS-87-11-1573, 1573-1584, 2006.

Prigent, C., F. Papa, F. Aires, W. B. Rossow, and E. Matthews, Global inundation dynamics inferred from multiple satellite observations, 1993-2000, J. Geophys. Res., 112, D12107, doi:10.1029/2006JD007847, 2007.

Prigent, C., E. Jaumouille, F. Chevallier, and F. Aires, A parameterization of the microwave land surface emissivity between 19 and 100 GHz, anchored to satellite-derived estimates, IEEE Trans. Geo. Remote Sens., 46, 344-352, 2008.

Saunders, R., M. Matricardi, and P. Brunel, An improved fast radiative transfer model for assimilation of satellite radiance observations, Quart. J. Roy. Meteor. Soc., 125, 1407-1425, 1999.

Seemann, S. W., E. E. Borbas, R. O. Knuteson, G. R. Stephenson, and H.-L. Huang, Development of a global infrared land surface emissivity database for applicationto clear sky sounding retrievals from multispectral satellite radiance measurements, J. Appl. Meteorol. Clim., 47, 108-123, 2008.

Weng, F., B. Yan, and N. C. Grody, A microwave land emissivity model, J. Geophys. Res., 106, 20115-20123, 2001.

Weng, F., and C. Liu, Satellite data assimilation in Numerical Weather Prediction models. Part I: Forward radiative transfer and jacobian modeling in cloudy atmospheres,J. Atmos. Sc., 60, 2633-2646, 2003.

Table I. The correlation matrix for uncertainties in the reference
SSM/I emissivity atlas for forested regions (class 1).

Channels	19V	19H	22V	37V	37H	85V	85H
SSM/I 19 GHz V	1.00	0.96	0.92	0.96	0.94	0.72	0.73
SSM/I 19 GHz H	0.96	1.00	0.90	0.95	0.95	0.71	0.72
SSM/I 22 GHz V	0.92	0.90	1.00	0.92	0.91	0.78	0.78
SSM/I 37 GHz V	0.96	0.95	0.92	1.00	0.96	0.79	0.79
SSM/I 37 GHz H	0.94	0.95	0.91	0.96	1.00	0.76	0.78
SSM/I 85 GHz V	0.72	0.71	0.78	0.79	0.76	1.00	0.93
SSM/I 85 GHz H	0.73	0.72	0.78	0.79	0.78	0.93	1.00

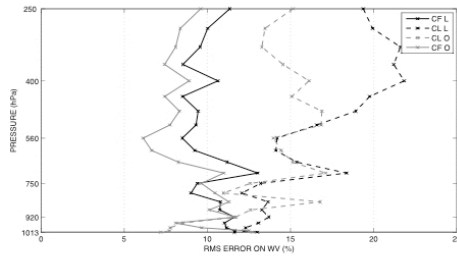Figure 3. The different steps in TELSEM, the microwave emissivity
calculator in RTTOV.

Figure 6. RMS relative error for the AMSR-E/HSB retrieval of
relative humidity (in %). The statistics are given over the Tropical
regions ($\pm30°$) for July 2002 and January 2003. Grey lines are for
ocean surfaces (O) and black lines for land (L). Continuous lines are
for Cloud Free (CF) scenes and dashed lines are for CLoudy (CL)
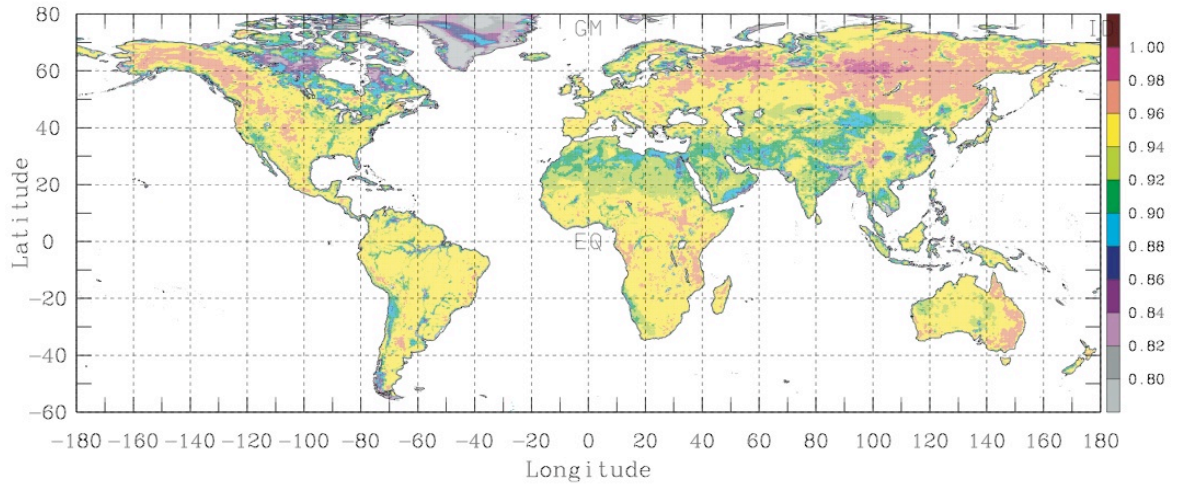situations.

Figure 1. Example of emissivity calculation with TELSEM for September at 31.4 GHz, for 15° incidence angle and vertical polarization.
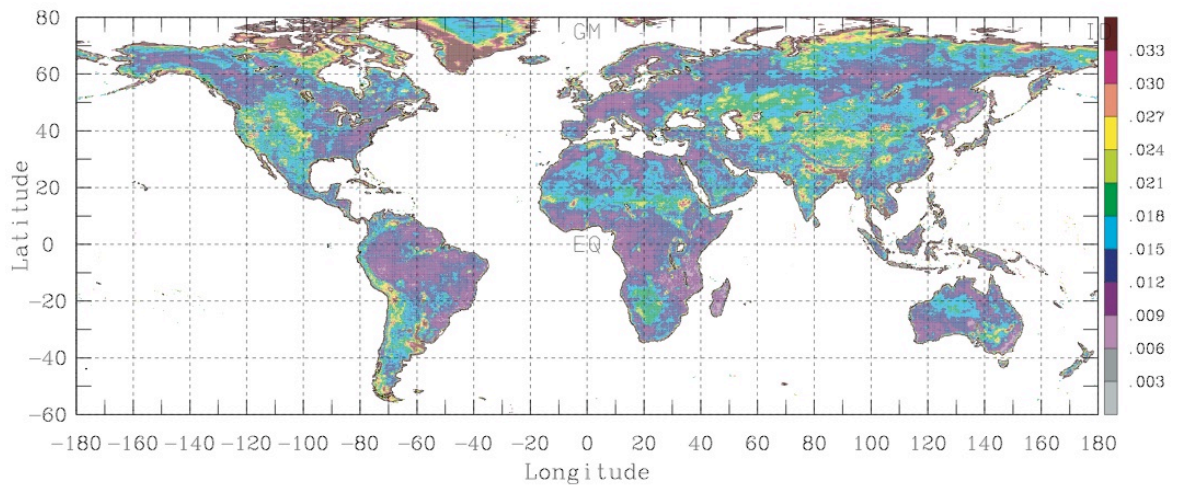

Figure 2. The emissivity uncertainty estimates for September, interpolated at 31.4 GHz, for the vertical polarization at 15° incidence angle.
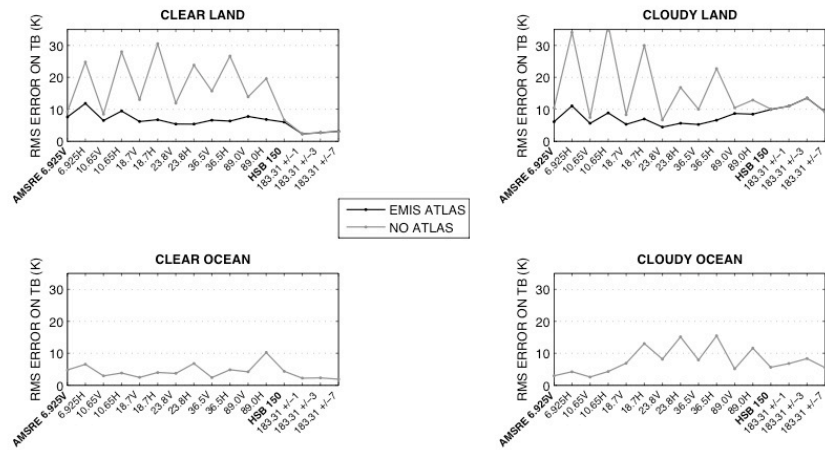
Figure 4. RMS errors between simulated and observed TBs for AMSR-E and HSB on board Aqua, for two months (July 2002 and January 2003), over the Tropics (±30° in latitude). Top left: over land for cloud-free situations; top right: over land for cloudy situations; bottom left: over ocean for cloud-free situations; bottom right: over ocean for cloudy situations. In black the simulations with the new emissivity model, in grey the original RTTOV simulations, using a fixed emissivity of 0.95.
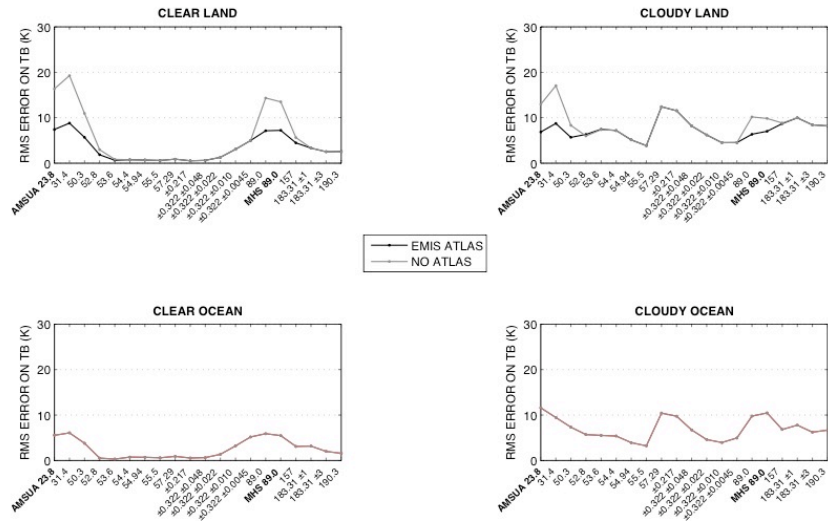

Figure 5. RMS errors between simulated and observed TBs for AMSU-A and MHS on board MetOp, for two months (July 2007 and January 2008), over the Tropics (±30° in latitude). Top left: over land for cloud-free situations; top right: over land for cloudy situations; bottom left: over ocean for cloud-free situations; bottom right: over ocean for cloudy situations. In black the simulations with the new emissivity model, in grey the original RTTOV simulations, using a fixed emissivity of 0.95.